University of Birmingham

School of Physics and Astronomy

Applications of Piezo Actuators for Space Instrument Optical Alignment

Author:
Michelle Louise Antonik
520689

30/03/2007

Supervisor:
Prof. Bruce Swinyard

Abstract

This report looks at an attempt to create a highly accurate passive alignment device that allows alignment to better than 1μm. It investigates the possibility of using piezo actuators as a method of achieving small movements to create this alignment device. The suitability of both photogrammetry and interferometry based systems has been studied. It has been concluded that photogrammetry based systems can only be used for alignment of up to 1.5μm. Interferometry based systems hold promise but further work is required to ensure their capabilities. The work required for this is detailed at the end of this report.

This report is 10093 words long.

Contents Page

Table of Contents

1 Introduction 1
1.1 Review of Current Alignment Techniques 1
1.1.1 Telescopic alignment 2
1.1.2 Photogrammetry 3
1.1.3 Laser Based Alignment 3
1.1.4 Interferometry 4
1.1.5 Fibre Optic Alignment 6
1.1.6 Overview and comparison of techniques 7
1.2 Camera Resolution 9
1.3 Fish Eye Lenses 10
1.4 Piezoelectricity and Piezo Actuators 11
1.4.1 Piezoelectricity 11
1.4.2 Piezo Actuators 13
1.5 Gray Values 13
1.6 Spatial and Temporal Fringe Patterns 14
2 Method Adopted 15
2.1 Apparatus Used 15
2.2 Techniques Used 17
2.2.1 Initial Calibration of Piezo Actuator 17
2.2.2 Original Design for Fine Calibration of Piezo Actuator 18
2.2.3 Interferometry Design for Fine Piezo Actuator Calibration 23
3 Results and Interpretation 26
3.1 Initial Rough Piezo Actuator Calibration 26
3.2 Fine Piezo Actuator Calibration 26
4 Future Work 31
5 Conclusions 32
6 Acknowledgements 32
7 References 366
8 Appendix 33

Table of Figures

Figure 1: The coordinate system used in this review. 2
Figure 2: Common targets in telescopic alignment. 3
Figure 3: Diagrammatic description of the Fresnel zone plate alignment technique. 4
Figure 4: A Michelson Interferometer 4
Figure 5: Constructive Interference 5
Figure 6: Deconstructive Interference 5
Figure 7: Interference pattern from a Michelson Interferometer 5
Figure 8: Input and output for a laser light source. 6
Figure 9: Input and output for a small range of frequenices. 6
Figure 10: The fibre optic sensor system brought for observing the structural changes of MIRI at cryogenic temperatures. 7

Figure 11: Table giving overview of alignment techniques researched. 9
Figure 12: Two peaks that are unresovlable. 9
Figure 13: Two peaks that are just resolvable. 9
Figure 14: Two peaks that are resolvable 9
Figure 15: Picture showing the relationship between D and Θ diagrammatically. 9
Figure 16: Picture showing the uncorrected effects of a fish-eye lens. 10
Figure 17: Picture showing a corrected image from a fish-eye lens....11
Figure 18: Shows two states of a ferroelectric crystal. 12
Figure 19: A non-ferroelectric crystal....12
Figure 20: Construction of a piezo actuator....13
Figure 21: Motion of piezo actuator 13
Figure 22: Temporal fringes 14
Figure 23: Spatial fringes caused by mirror misalignment....14
Figure 24: Picture of the rough calibration of the piezo actuator. 15
Figure 25: Initial set-up for the fine calibration of the piezo actuator. 15
Figure 26: Picture of the second fine calibration set-up. 16
Figure 27: Picture of the third fine calibration set-up. 16
Figure 28: Initial calibration of the webcam. 17
Figure 29: Second calibration of the webcam. 17
Figure 30: Original method of fine piezo calibration. 18
Figure 31: Plot in ImageJ of the brightness of an image 19
Figure 32: Graph showing the calibration data for the initial calibration of the webcam. 20
Figure 33: Geometry relating the distance moved across the CCD to the distance moved by the mirror....20
Figure 34: Graph showing the movement of the laser beam across the CCD. 21
Figure 35: Plots of data points with Gaussian curves fitted....22
Figure 36: Graph showing the movement of the average centroid peak across the central portion of the CCD. 22
Figure 37: Incident rays on the CCD 23
Figure 38: A diagram of the Michelson interferometer used....24
Figure 39: Diagram of the adapted Michelson interferometer....25
Figure 40: Graph showing the results of the change in step size as a function of the number of steps from the start. 26
Figure 41: Graph showing the position of zero path difference. 27
Figure 42: Graph of the zero path difference area. 27
Figure 43: Manufacture's results for the movement of the piezo actuator. 28
Figure 44: Graph showing the zero path difference area with a small sample rate. 28
Figure 45: Graph of resultant when a background image is removed from an image taken inside the zero path difference area. 30
Figure 46: Cross section through the incident light. 30
Figure 47: Area over which the integrated density was taken. 30
Figure 48: Zero path difference area looked at using a small sample rate and the integrated density. 31
Figure 49: Set-up required for the cryogenic calibration of the piezo actuator. 32

1 Introduction

Over the years the Hubble Space Telescope has given the scientific community many amazing pictures. However, it is now rapidly coming to the end of its life and so a new telescope is needed to replace it. This will be done by the James Webb Space Telescope (JWST) due to launch in 2013[1]. The JWST will carry several instruments including MIRI, a mid infrared instrument that looks at wavelengths of light between 5 and 27μm[2]. It is designed to be able to see through dust and gas clouds which absorb radiation in the near infrared and optical regions, which current instruments use. Rutherford Appleton Laboratories have been contracted to determine what structural changes occur during operation at cryogenic temperatures as MIRI's operating temperature will be approximately 7K.

The measurement of deformation due to cryogenic temperatures is to be done using fibre optic sensors. These are commercially brought sensors that have a trade off between their range of detection and the accuracy to which data is taken. Data needs to be able to be taken over a range of 3cm but these fibres do not give an ideal accuracy of 1μm[3], as any smaller movement becomes lost in high frequency cryogenic noise. It is known that fibres with a shorter detection range have accuracies of 2.5μm, giving rise to the possible potential for the accuracy of the longer ranged fibres to be increased. This project aims to investigate the use of the piezo actuator's nanometre movements as a method of being able to increase the accuracy of the fibre optic sensors. The piezo actuator needs to be calibrated so its movement becomes repeatable and predictable. The fibre optic sensor can then be reflected off the piezo actuator and the actuator moved in small stages. If a small known change in the actuator's position is accompanied by a repeatable change in the fibre's output then these results can be used for finer calibration of the sensor, generating better results when the instrument is in orbit.

1.1 Review of Current Alignment Techniques

The precise alignment of components within instruments is often needed to very high tolerances. To ensure proper alignment within instruments there are a number of common alignment techniques which fall into two categories: active and passive alignment. Active alignment was developed for aligning fibres where an extremely high tolerance is required. For this method the equipment needs to be powered and so generates large amounts of noise, which can cause disruption in sensitive environments. Passive alignment can be divided into two categories. These are mechanical and optical alignment. Mechanical alignment can use either mechanical stops to lock parts in place or the surface tension from solder which pulls parts into place[4]. This review focuses on the optical alignment techniques.

There are three main types of optical alignment: telescopic, photogrammetry and laser based alignment. Telescopic alignment uses a series of lenses to allow the deviation of a target from a given line of sight to be measured. Photogrammetry involves using one or more cameras to triangulate the position of a given object. Laser based alignment involves reflecting a laser off the object and then detecting either misalignment within the beam or a change in the intensity of the beam. Misalignment of the laser beam on a target is usually used for ensuring alignment whereas a change of beam intensity is more commonly used for distance measurements.

There are six degrees of freedom in which misalignment can occur. These are in the axial directions and in the rotational directions, around each of the axes. The coordinate system has been taken to be as shown in figure 1, where pitch is around the y-axis, yaw around the x-axis and roll around the z-axis.

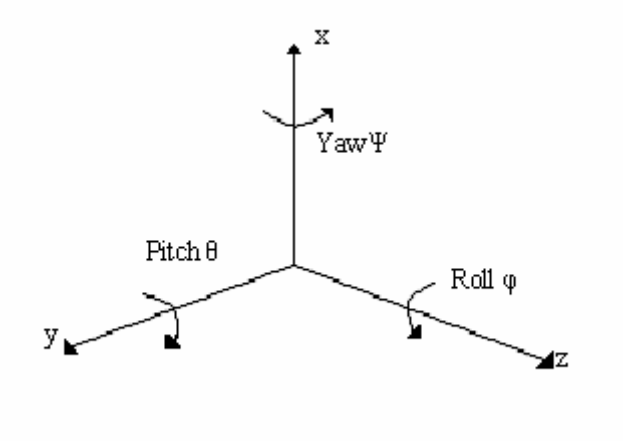

Figure 1: The coordinate system used in this review.[5]

In this review, short explanations on the basic principles of each main alignment technique are given. Variations on a technique will give different accuracies and so the specific techniques researched are compared in a table in figure 11. The technique that is appropriate to use varies depending on circumstances. For the cryogenic testing of MIRI the use of fibre optic sensors had already been decided upon as they use simple equipment with a high accuracy that can be fed into the cryostat allowing the electronics to remain outside, reducing noise levels.

1.1.1 Telescopic alignment

There are two main components to a telescopic alignment setup. These are the telescope and the target[6]. The telescope is placed with the observer and the target is placed at the opposite end of the distance to be measured. The target is centred on where the line of sight should be. By looking through the telescope the target can be seen. If the target is in the correct place the central markings on the target should overlap with the cross hairs on the telescope. This allows the distance between the target and its ideal placement to be measured. This technique can only be used over large distances but it does give results that can be accurate up to 0.008mm.

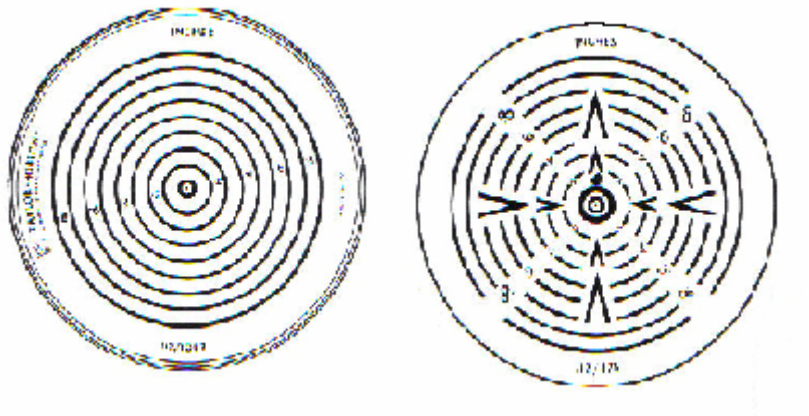

Figure 2: Common targets in telescopic alignment.

1.1.2 Photogrammetry

Photogrammetry uses cameras to determine the position of an object by looking at the placement of the object on the 2D image that is produced. The position of the image in the camera's coordinates corresponds to the object's position in the world coordinate system. In order to do this complicated mathematics are involved that will not be gone into here due length constraints, however, a good overview was written by Salvi *et al* (2002)[7].

The distortion from the lenses used in photogrammetry is taken into account within the alignment techniques. If the distortion was not taken into account then the images received would give inaccurate positions of objects. However for high distortion lenses, extra calibration may be required. Other cameras are designed to move and so the placement of the camera needs to be known before other distances can be calculated.

1.1.3 Laser Based Alignment

A very common laser based system to use is often similar to that employed by Ayliffe *et al* (2001). Here a laser with a wide, collimated and monochromatic beam is incident on optoelectronic-VLSI (OE-VLSI) chips. On the periphery of the OE-VLSI chips are off-axis liner Fresnel Zone Plates (FZP). As a single linear FZP will focus the light into a line, by having two FZP oriented at 90° with respect to each other a cross pattern is generated at the focal plane. Because the FZPs are off axis the cross pattern will shift as it is imaged at different points along the optical axis. The placement of the cross pattern with respect to the chrome alignment targets are noted by a CCD. Only three pairs of FZPs are necessary as the cross patterns give information on the axial position as well as the rotational position. The largest error occurs when the incident light is not perfectly orthogonal to the OE-VLSI chip. This causes a lateral shift of the optical crosses with respect to the alignment targets. Other sources of error come from improper judgement of when the optical cross is properly centred and from the accuracy of the processes used to create the FZPs, although this is usually negligible.

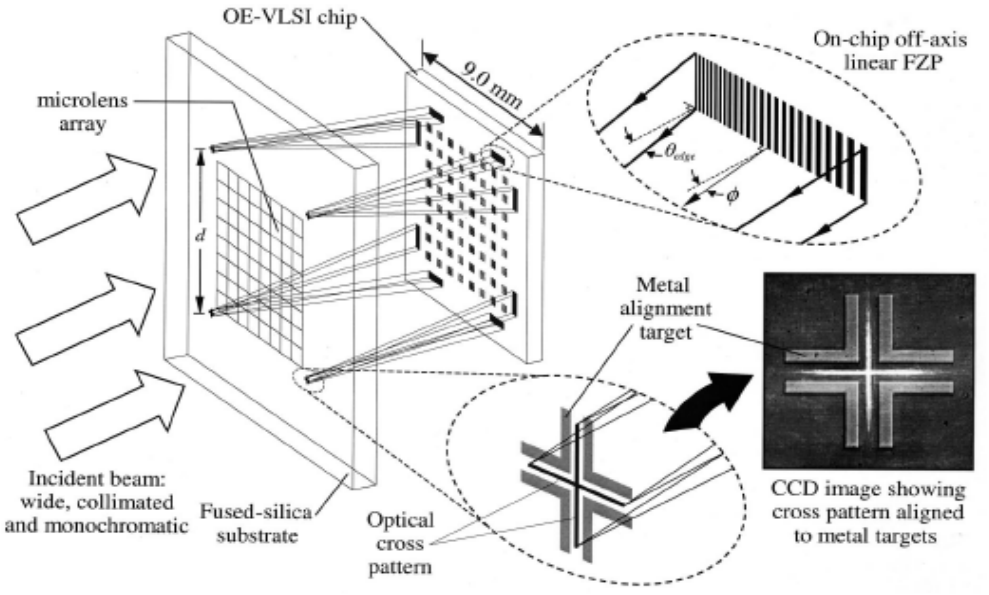

Figure 3: Diagrammatic description of the Fresnel zone plate alignment technique. [8]

1.1.4 Interferometry

Interferometry allows alignment by the use of interference patterns caused by the superposition of two or more electromagnetic waves on top of each other. As these waves originated from the same source and were divided by a beamsplitter, they should remain in phase with each other making it is possible to find the difference in the distance travelled by the waves using the difference in their phase. If the phase is the same then one beam of light has travelled an exact number of wavelengths more than the other wave. The accuracy of this technique is very high as it measures to a fraction of the light wavelength. One of the most common and simplest methods is the Michelson Interferometer, shown in figure 4.

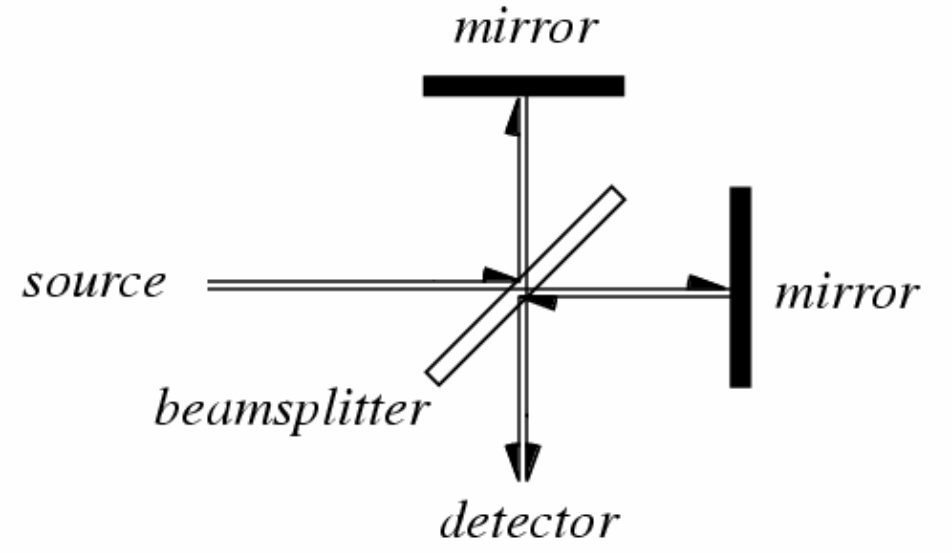

Figure 4: A Michelson Interferometer. Arrows show the direction of travel of the light[9]**.**

The Michelson interferometer works by sending a coherent light source into a beamsplitter. This splits the light into two beams of equal intensity. Each beam goes

down a separate arm of the Michelson and is reflected back to the beamsplitter. Beamsplitters are often half-silvered mirrors with a very sparse coating of the reflective molecules, about half needed for a fully opaque mirror to be created. This allows half of the light hitting the half silvered mirror to pass through and reflects the other half as a normal mirror would[10]. The beams are recombined by the same mechanism so only fifty percent of the light entering the Michelson reaches the detector. If the distance between the two mirrors is different then interference will occur when the two beams are recombined due to changes in the phase of the laser beam.

For constructive interference the equation

$$pd = m\lambda \tag{1}$$

must be satisfied, where pd is the path difference between the two arms of the interferometer, m is an integer and λ is the wavelength of light used. As a whole number of wavelengths has passed the waves remain in phase with each other. If the condition

$$pd = m\lambda / 2 \tag{2}$$

occurs then the waves are exactly out of phase with each other causing deconstructive interference to occur. These effects can be seen below in figures 5 and 6.

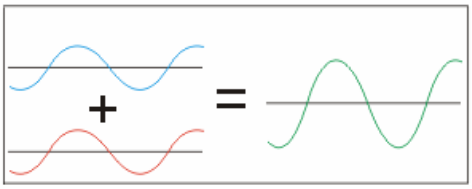

Figure 5: Constructive Interference[11]

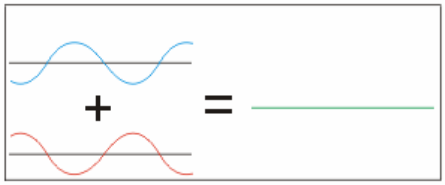

Figure 6: Deconstructive Interference

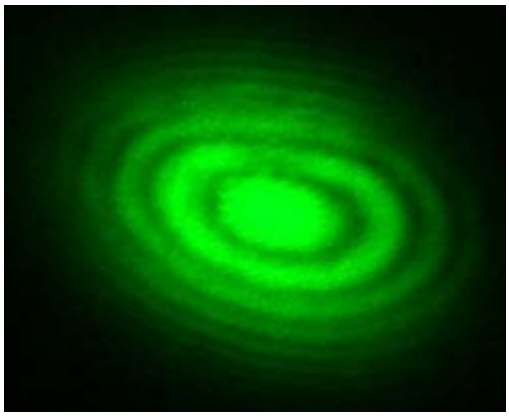

Figure 7: Interference pattern from a Michelson Interferometer. Bright rings arise from constructive interference occurring and dark rings from deconstructive interference occurring[12].

Light will only create the interference pattern over a given length of space. It is over this distance that the light remains in phase with itself and so can cause constructive and destructive interference. This length is called the coherence length[13] and is given by

$$\Delta l_c = \frac{c}{\Delta \upsilon}, \tag{3}$$

where Δl_c is the coherence length, c is the speed of light and Δv is the range of frequencies used. By increasing the number of wavelengths entering the

interferometer the range of frequencies is increased and so decreases the coherence length.

A Michelson generates the interference pattern by Fourier transforming the input. For a laser where the input is represented by a single frequency, as seen in figure 8, the output becomes very narrow and well defined. If a larger range of frequencies is used then the output becomes larger although it generates a more complicated pattern. This comes from each frequency giving an output of a cosine wave which then add together to form a sinc function. The diagram in figure 9 shows the output for a small range of frequencies, e.g. the red wavelengths of light. For a more complicated input, e.g. white light, several fringe patterns would be outputted, e.g. the red frequencies would interfere with each other as would the green and the blue frequencies.

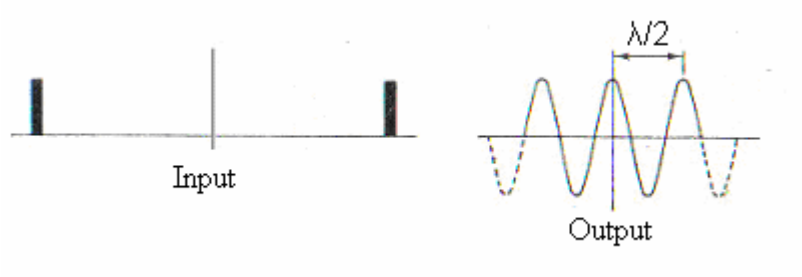

Figure 8: Input and output for a laser light source[14].

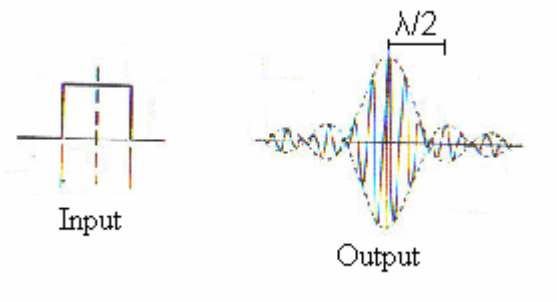

Figure 9: Input and output for a small range of frequenices.

The accuracy of a Michelson interferometer tends to be taken to half of the wavelength of light used as it is at this point that a ring will disappear giving an unambiguous point of reference for the change of distance of the arm. However by using a high sampling rate in a low noise system it possible to detect small changes in the intensity of the output. Using this technique it has been possible to achieve accuracies of less than 1nm[15]. This makes interferometry the most accurate of all the alignment techniques.

1.1.5 Fibre Optic Alignment

Whilst technically an active technique as it is a powered system, the fibre optic sensors become effectively a passive alignment system at the measurement end. This is achieved by sending a laser beam down a long fibre optic cable allowing all electronics to be kept away from sensitive areas and so reduces noise. Measurements are taken by the laser beam emerging from the end of the fibre and reflecting off a surface, back into the fibre and returning down the cable[16]. The displacement of an object can be found by the intensity of the returning light which varies proportionally to the distance between the end of the sensor and the object.

The accuracy of this method is dependant on the range over which the fibre is capable of taking results, with the longer range fibres having the least accuracy. Whilst this method does not give the most accurate results, as compared to other laser methods, and only has a narrow angle range over which it can be used, it has the advantage that it is flexible and portable with the ability to be used within a vacuum and at cryogenic temperatures with ease. This allows measurements in areas that are noise sensitive, such as the cryostat that MIRI will be in. These fibres have the disadvantage that coiling increases internal reflection and so by coiling them too tight (that which has a bend radius less than 25mm) causes the sensor to fail.

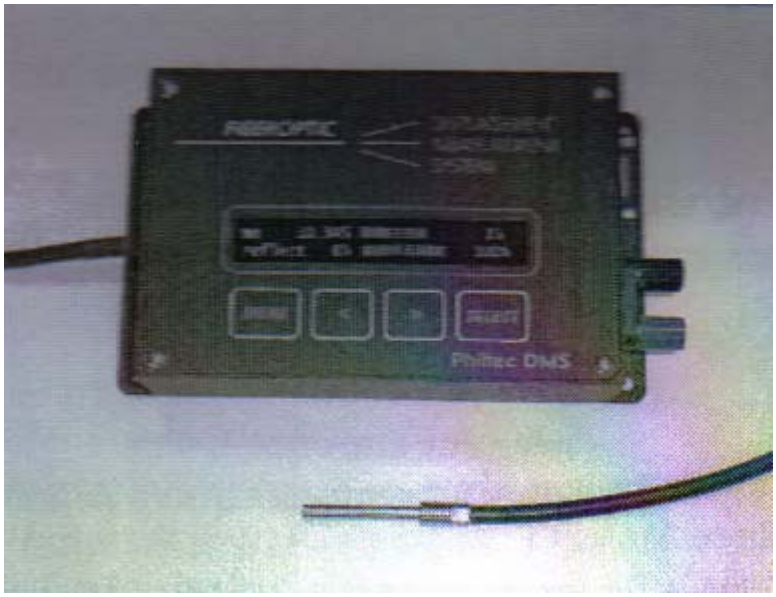

Figure 10: The fibre optic sensor system brought for observing the structural changes of MIRI at cryogenic temperatures.

1.1.6 Overview and comparison of techniques

The table below gives common accuracies and ranges of the more widely used methods of alignment. It also gives the main advantages and disadvantages of each technique. These factors need to be considered when deciding upon an alignment system to ensure the most appropriate method is used for a given situation.

Technique	Range	Accuracy	Main Advantages	Main Disadvantages
Telescopic Alignment	1m – 30m	±0.008mm (at 1m) to ±0.05mm (at 30m)	Allows accurate readings over large distances. Easy to use.	Only works over large distances. Need exact positioning of the line of sight. Interference subjective to operator.
Photogrammetry: Hall Method[17]	Not Given	±0.5634mm	Simple and fast technique.	Uses ineffective calculating techniques

Photogrammetry: Faugeras Method	Not Given	±0.1694mm	Fairly simple technique.	Needs an initial guess to start calculations.
Photogrammetry: Tsai's Method	Not Given	±0.1578mm	Reduces calculation parameters and hence time of calculation.	Camera parameters need to be known.
Photogrammetry: Weng's Model	Not Given	±0.1696mm	Can compensate of three types of lens distortion.	Complicated model with time consuming calibration. At least five test points needed for calculation of position.
Photogrammetry: Zhang and Pan (2004)[18]	Up to 266mm	±0.487mm	Manoeuvrable and portable. Gives direct control over where images are taken.	Need multiple images for good accuracy.
Photogrammetry: Iovenitti *et al* (1996)[19]	Must stay at the focal length of the camera	±0.879mm	Manoeuvrable and easily modelled.	Possibility of recalibration needed during the taking of results.
Laser Based Alignment: Ayliffe *et al* (2001)	N/A. Distance is set by the equipment used.	Axial x and y: ±3μm Rotational x and y: 0.022° Axial z: ±13μm Rotational z: 0.023°	Technique is compact and is sensitive to all six degrees of freedom.	Can only tell that the alignment is not correct, not which degree of freedom is out.
Laser Based Alignment: Châteauneuf and Kirk (2004)[20]	N/A. Distance is set by the equipment used.	Axial x and y: ±5μm Rotational x and y: 0.007° Axial z: ±20μm Rotational z: 0.036°	Gives measurement of misalignment independently of the other degrees of freedom.	Requires five pairs of alignment features.
Laser Based Alignment: Li *et al* (2005)[21]	±30°	±0.005°	Accurately measures the roll. Remains stable in temperature and magnetic field fluctuations. Uses a cheap light source and simple equipment.	Only measures the roll. Calibration is needed before every measurement.
Laser Based Alignment: Liu *et al* (2004)[22]	Rotational x: ±2° Rotational y and z: ±0.1°	Rotational x and z: ±0.1° Rotational y: ±0.05°	Simple procedure without lots of equipment.	Very small range.

Laser Based Alignment: Jahns and Däschner (1992)[23]	N/A. Distance is set by the equipment used.	±0.6µm	Allows very precise measurement.	Error easily introduced.
Fibre Optic Sensors	Either 5.1mm, 12.7mm or 30mm	±1.25µm, ±3.8µm, ±3.1µm	Removes all electronics from the measurement area.	Coiling of fibres degrades performance.

Figure 11: Table giving overview of alignment techniques researched.

1.2 Camera Resolution

The limit at which two objects can be distinguished is when the peak of one signal is central on the first diffraction minimum as is shown in figure 13. If the signal peaks are any nearer then they start to merge creating one large signal peak.

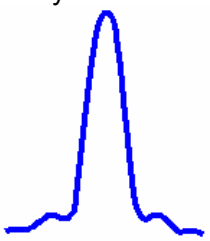

Figure 12: Two peaks that are unresovlable[24].

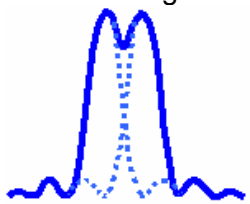

Figure 13: Two peaks that are just resolvable - they are at the Rayleigh's Criterion.

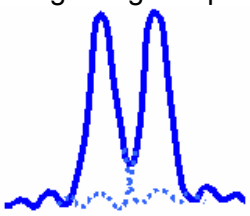

Figure 14: Two peaks that are resolvable

This limit is the resolution of the camera and is the minimum distance needed between two objects to be able to distinguish them as separate entities. This distance is given by the Rayleigh Criterion,

$$\theta = \frac{1.22\lambda}{D}, \tag{4}$$

where Θ is the angle between the two objects, λ is the wavelength of light used and D is the diameter of the lens, as shown in figure 15. In equation 4 the small angle approximation is used to allow Θ to replace sinΘ.

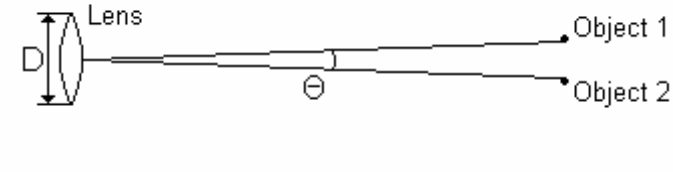

Figure 15: Picture showing the relationship between D and Θ diagrammatically.

The detector is placed at the focal point of the lens. The pixels on the CCD may be larger than the resolution of the camera but by using curve fitting software it is possible to fit a Gaussian curve that has a well defined peak to the received signal allowing the placement of the signal peak to be placed to better than one pixel. This allows large pixels to be used with the camera remaining diffraction limited.

1.3 Fish-Eye Lenses

Fish-eye lenses are used in webcams to allow a small CCD with a small lens to collect light from a larger than otherwise possible area and so image a large area[25]. The image taken is highly distorted as can be seen below in figure 16. This distortion is automatically processed out by the webcam's software giving the image as would been seen by the naked eye shown in figure 17.

Figure 16: Picture showing the uncorrected effects of a fish eye lens.

Figure 17: Picture showing a corrected image from a fish eye lens.

Due to the wide angled lens, light from a given position is concentrated onto a small part of the CCD. Any small change in position of an object is difficult to detect in the image as the change on the CCD is very small. By removing the lens the ratio of movement along the CCD to that along the image is returned to 1:1. However, the webcam can no longer be used to take images of anything other than a pin point light source as the software for compensating for the fish eye lens remains running.

1.4 Piezoelectricity and Piezo Actuators

1.4.1 Piezoelectricity

Piezoelectricity is an electric polarity that results from a stress being applied to a dielectric crystal[26]. These crystals usually do not conduct electricity but the molecules within them can easily be rearranged under pressure and this then causes the polarity by either ferroelectric or non-ferroelectric means.

If a crystal is ferroelectric this means that it has two or more stable orientations that the atoms can be in when no stresses are applied[27]. A mechanical stress will force the atoms from one stable state to another. As the particles are arranged differently in the different stable states it follows that the overall polarity of the crystal changes

with the state. A diagram of this is shown below in figure 18. Conversely, by applying an electric field to the crystal a polarization is induced which forces the particles to align themselves with it and so forcing them into a different orientation. In this orientation the particles have different spacing and the crystal size changes.

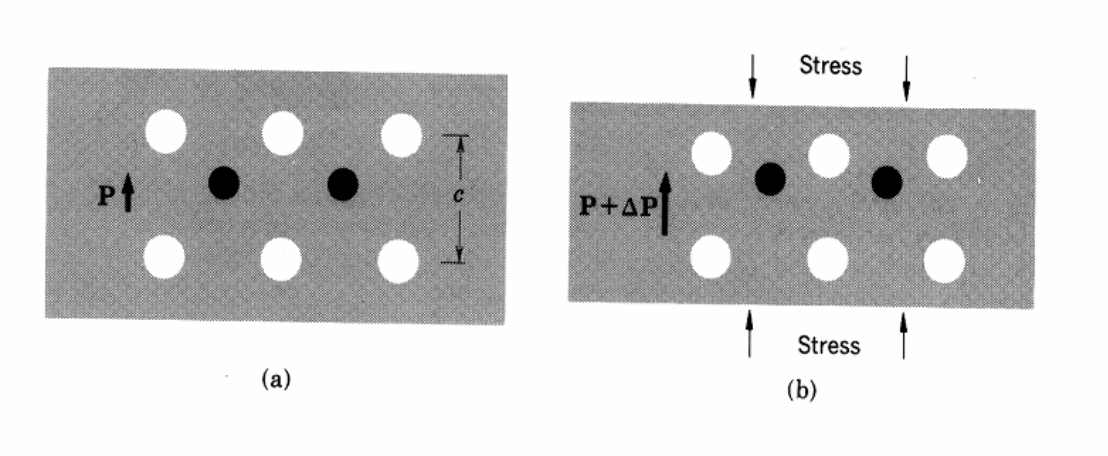

Figure 18: Shows two states of a ferroelectric crystal. The white dots represent ions and the black dots represent electrons. In (a) it initially has a polarization of P across it. In (b) a stress is applied forcing the ions to move closer than their initial spacing of *c*. The electrons remain in their original position so giving a new polarization across the crystal of P+ΔP.

A non-ferroelectric crystal only has one stable state but both a mechanical strain and an electric field can cause a stress across the crystal which distorts it. This occurs because the unstressed crystal has a three-fold symmetrical axis where the three dipole moments have a sum at the vertex of zero. When a stress is applied to the crystal it compresses it distorting the dipole moments. This leads to polarization about one axis, as shown in figure 19, due to the dipole moments no longer cancelling each other out at the vertex.

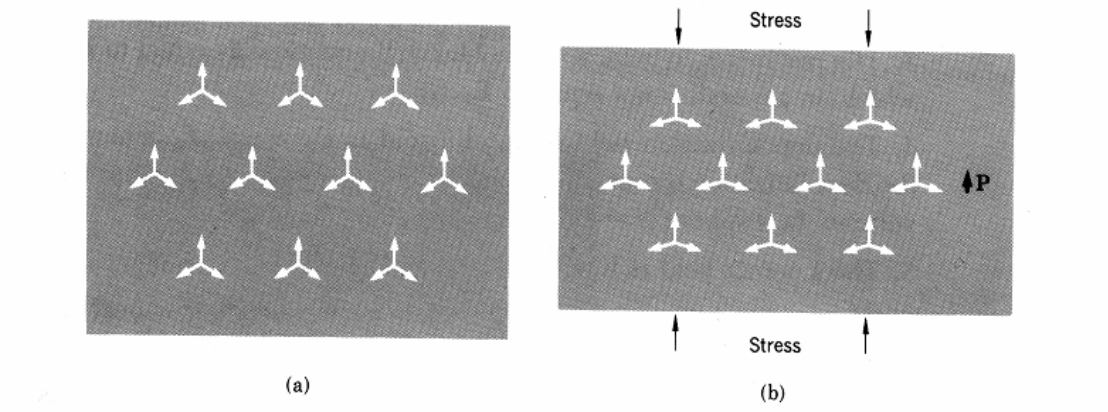

Figure 19: A non-ferroelectric crystal. The arrows symbolises the dipole moments. In (a) they cancel each other out and so there is no overall polarization and in (b) where the stress has compressed the crystal the dipole moments are deformed, creating and overall polarization of P.

The relationship between the mechanical stress and the electric field on the polarization and the elastic strain of the crystal is seen in the one-dimensional equations for piezoelectric crystals. As can be seen in equation 5,

$$P = Zd + EX, \tag{5}$$

the polarization (P) is determined by the stress (Z) and the electric field (E). This is the same for the elastic strain (e) (which determines the size of the crystal) where

$$e = Zs + ED, \quad (6)$$

although different constants are used here meaning the polarisation and the elastic strain are affected by different amounts. For the polarization, d is the piezoelectric strain constant and χ is the dielectric susceptibility of the crystal. In the elastic strain equation s is the elastic compliance constant and D is the piezoelectric strain constant.

1.4.2 Piezo Actuators

Piezo actuators are based around piezoelectric crystals. The basic construction and movement of an actuator is given below.

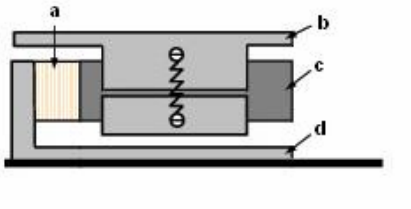

Figure 20: Construction of a piezo actuator. (a) Piezoelectric crystal (b) Sliding block (c) Guiding rod (d) Fixed base[28]

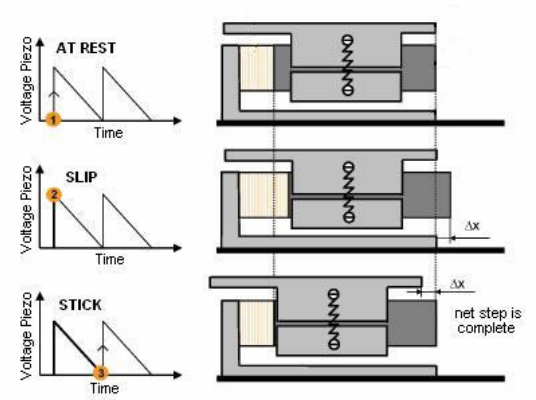

Figure 21: Motion of piezo actuator. Graphs at side show the voltage supplied to the piezo over a given time. Yellow dot marks the piezo actuator's position.

The piezoelectric crystal is attached to a fixed base and the guiding rod. This means that all of the piezoelectric crystal's movement is forced into moving the guiding rod rather than moving the whole assembly. The sliding block rests on the guiding rod and is not fixed so only fiction stops it from moving. The movement of the piezo actuator is controlled by the piezoelectric crystal. A fast expansion of the crystal by a sudden increase in voltage forces out the guiding rod quickly, overcoming the frictional forces so leaving the sliding block in its original position. A slow voltage decrease gives a slow contraction of the piezoelectric crystal. This smaller force is not enough to overcome friction and so the sliding block is pulled back with the guiding rod, creating a net step. This process can be repeated thousands of times for a large overall movement and is only limited by the length of the guiding rod. It is known as slip-stick motion.

1.5 Gray Values

Gray value is a measure of the brightness of a colour as a shade of grey. It ranges from 0 (black) to 256 (white). These levels have been chosen as they allow the coding to take place in 8 bytes, allowing for ease in programming. A colour image is converted to grey by using 30% of the red value, 59% of the green value and 11% of the blue value[29]. These percentages used were chosen to mimic the human eye's sensitivity to colour.

1.6 Spatial and Temporal Fringe Patterns

Fringe patterns occur when two coherent electromagnetic waves overlap. If both the polarisation and the phase of the two waves are exactly aligned then constructive interference takes place where the two waves combine to form one large wave. If the polarisation and phase of the waves are exactly out of phase then complete destructive interference occurs and the two waves cancel each other out. A fringe pattern is a series of this constructive and destructive interference. As the light originated from the same source at least one of the waves has to be altered in some way for the fringes to occur. This can happen either spatially or temporally. Temporal fringes come from one of the waves being delayed e.g. by moving one mirror further back so it has to travel further before it's reflected.

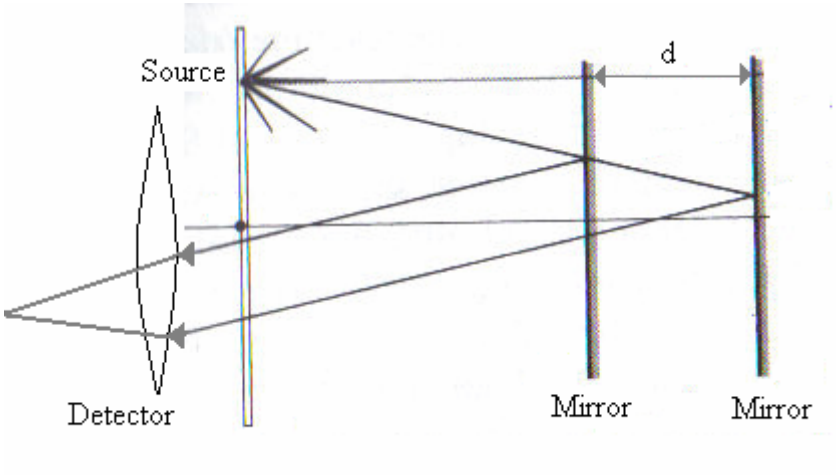

Figure 22: Temporal fringes. The bottom light ray takes 2d longer to reach the detector, time delaying it.

Spatial fringes occur when a copy of the wave has been shifted within space, and so this causes interference. A picture of this occurring due to misalignment of the mirrors is shown in figure 23.

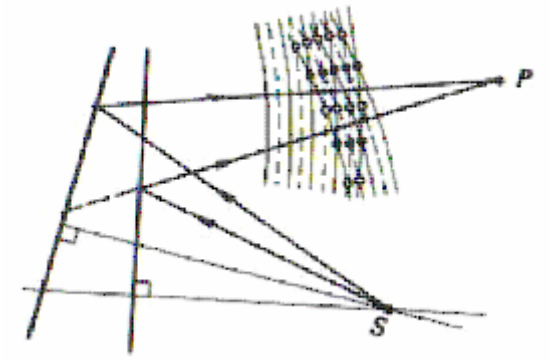

Figure 23: Spatial fringes caused by mirror misalignment. White dots give position of complete deconstructive interference and black dots give position of complete interference.

2 Method Adopted

2.1 Apparatus Used

Several calibration experiments were undertaken each requiring different equipment. A picture is given of each set-up with a large scale picture of each piece of equipment given in the appendix.

The initial calibration was for a rough calibration of the piezo actuator and consisted of using the piezo actuator and a linear voltage displacement transducer (LVDT) probe as shown in figure 24. Here (a) is the LVDT probe and (b) is the piezo actuator.

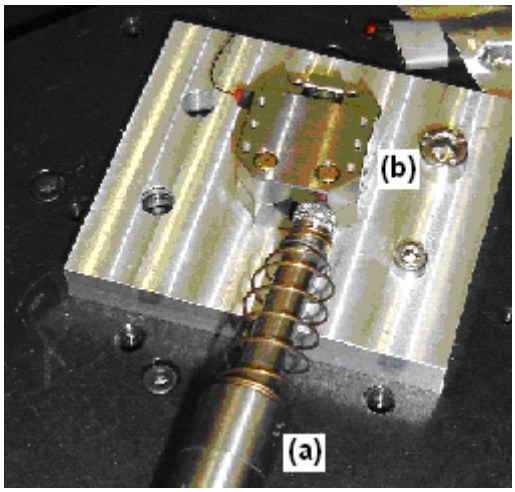

Figure 24: Picture of the rough calibration of the piezo actuator.

The second method involved trying to create a fine alignment system for the calibration of the piezo actuator. Here a class IIIa laser (c) was used to reflect a laser beam off a mirror mounted on the piezo actuator by means of an aluminium bracket (e). The light was reflected into a Phillips PCVC840K ToCam (d).

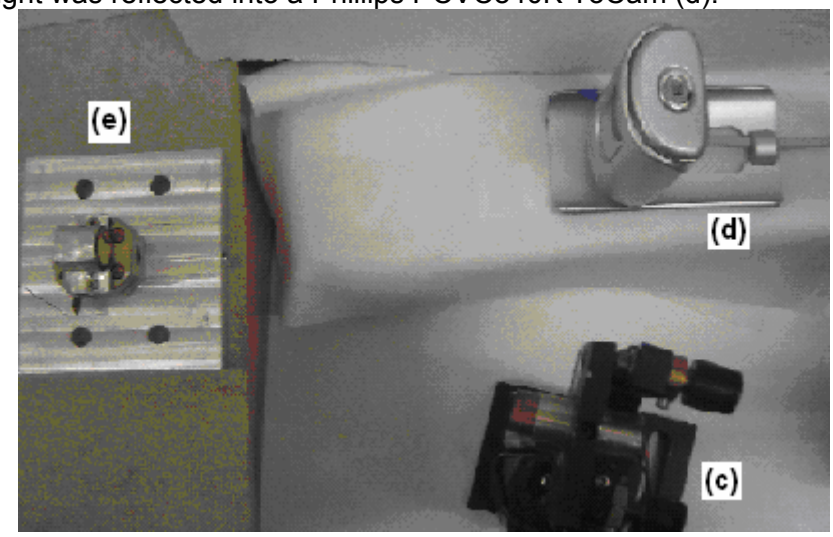

Figure 25: Initial set-up for the fine calibration of the piezo actuator.

The third method, again for the fine alignment of the piezo actuator, comprised of a Michelson interferometer with the piezo actuator as the mirror at the end of one arm. Its set-up is as given in figure 26 where (c) is the laser source, (f) a beam expander, (g) ground glass, (h) a polariser, (i) an iris, (j) a beamsplitter, (e) is the piezo actuator with a mirror mounted on top, (k) is a full silvered mirror, (l) a focusing lens and (d) is the webcam.

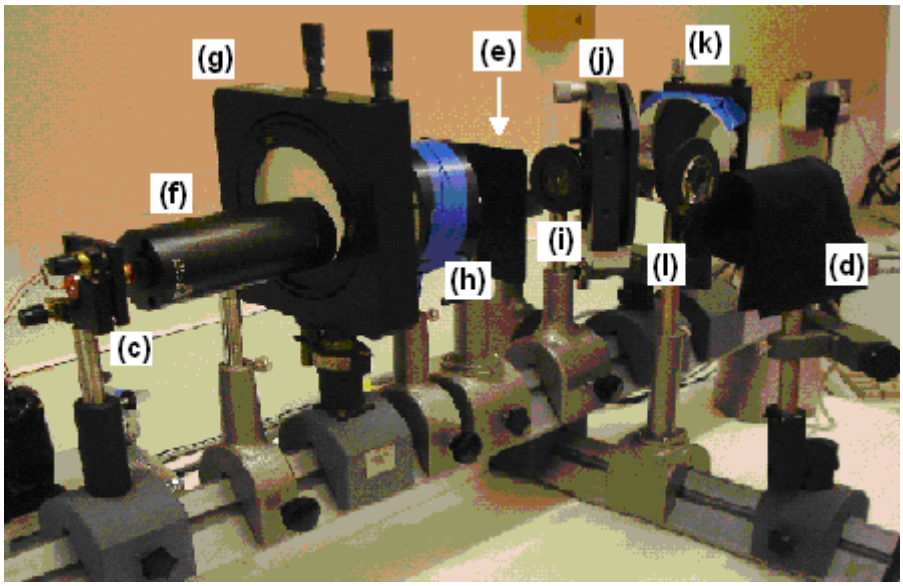

Figure 26: Picture of the second fine calibration set-up.

This was then adapted with the laser source being replaced by (m) a red light source and the polariser and ground glass being replaced by a second iris (n).

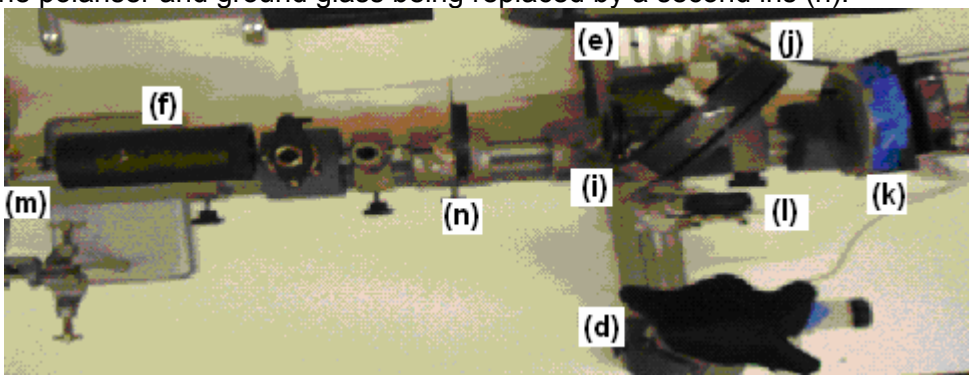

Figure 27: Picture of the third fine calibration set-up.

The webcam was calibrated using two methods. Firstly by a light source (o) on a sliding plate (p), figure 28, and secondly by a laser source (c) moved across the webcam's CCD (d), figure 29.

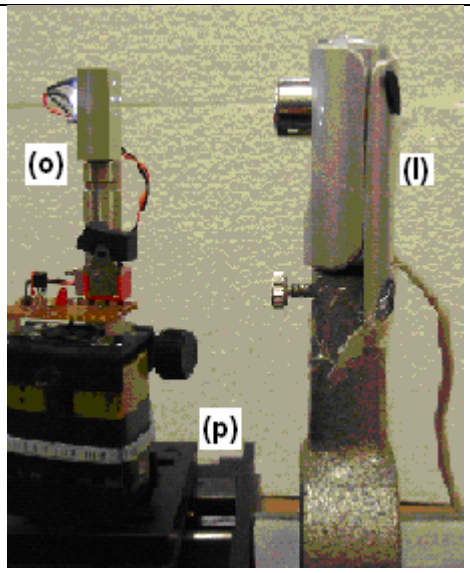

Figure 28: Initial calibration of the webcam.

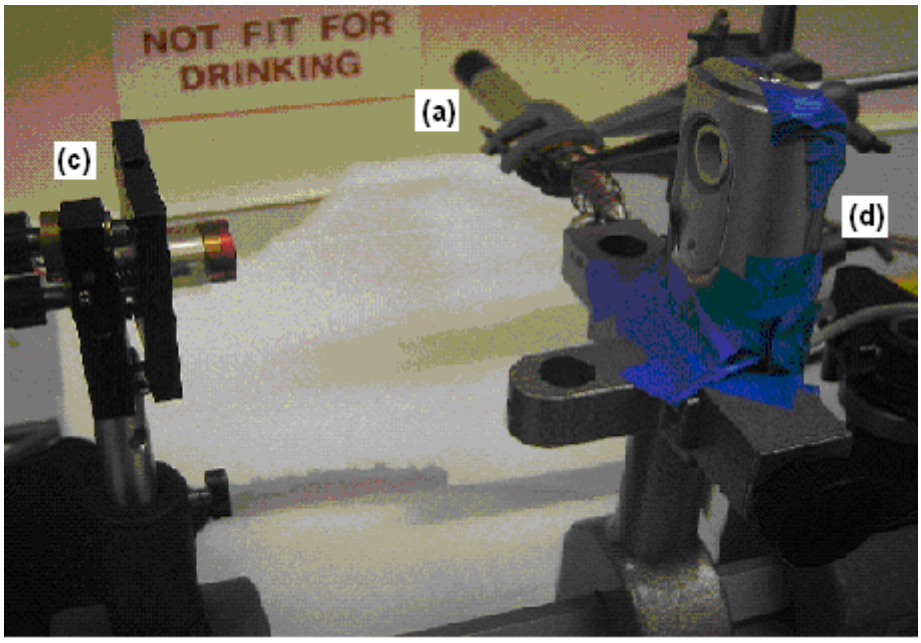

Figure 29: Second calibration of the webcam.

2.2 Techniques Used

2.2.1 Initial Calibration of Piezo Actuator

The first stage in this project was the rough calibration of the piezo actuator. This was needed to ensure that the piezo actuator was working within its normal parameters at room temperature and to get a feel of the motion it's capable of as initially its step sizes were unknown. This was achieved by placing a LVDT probe directly against the actuator. As the piezo actuator moved outwards it pushed in the

LVDT probe which registered the change in position. This set-up has been shown in figure 24.

The piezo actuator was moved in groups of fifty steps between each position reading as this was the smallest number of steps that gave a measurable change every time on the LVDT's output. The piezo actuator is controlled through an ANC150 controller which allows computer control through software called TerraTerm.

2.2.2 Original Design for Fine Calibration of Piezo Actuator

The original fine alignment system was based around photogrammetry techniques and is also discussed in the paper submitted with this report. A webcam was used as the detector and once pictures were taken geometry was then used to determine distances. The set-up was as in figure 30 were the laser is incident on the mirror mounted on the piezo actuator at an angle which then reflects into the webcam's CCD.

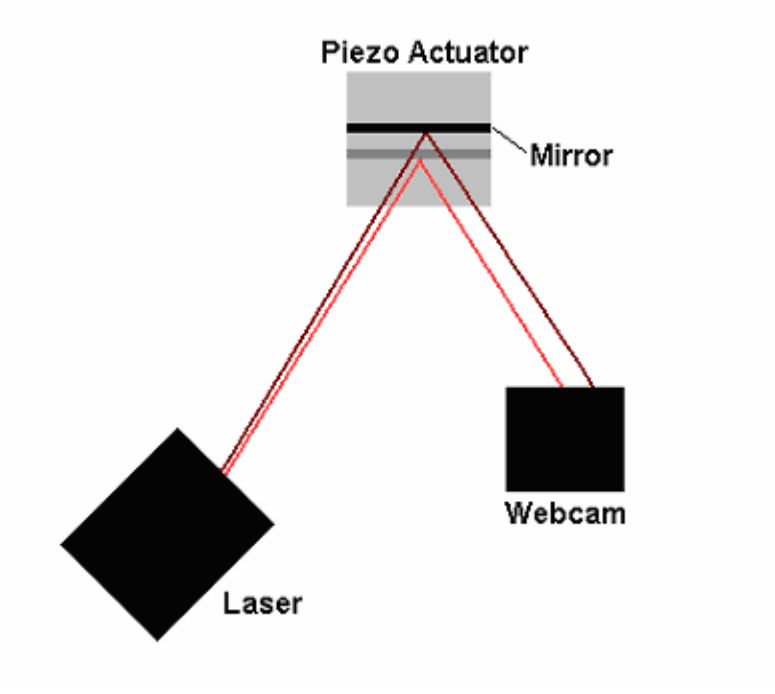

Figure 30: Original method of fine piezo calibration.

The webcam was linked to a computer where the images were processed using the freeware program ImageJ. This program allowed a cross section to be taken through the image at a fixed point allowing all the images to be compared at the same position. They were analysed for brightness and displayed in a graphical form as can be seen in figure 31.

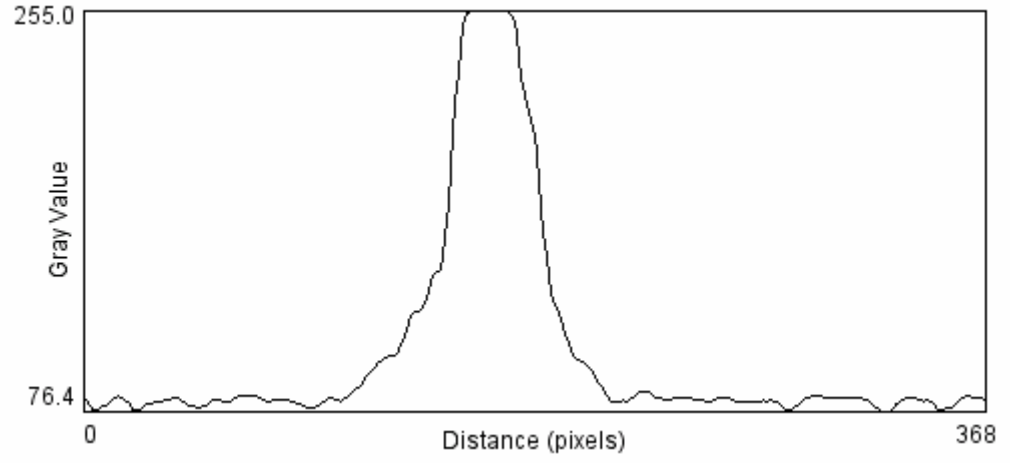

Figure 31: Plot in ImageJ of the brightness of an image. Brightness is plotted as a Gray Value along the y-axis and pixel distance is along the x-axis

The brightness is plotted against the distance along the CCD as a number of pixels. This allows any shifting of peaks to be seen easily and qualitatively. In order to be able to relate the pixel distance in the graph to an actual movement of the piezo actuator a calibration of the webcam needed to be done.

The webcam's calibration set-up was shown in figure 28. The light source is mounted on a sliding plate controlled by a micrometer so it can be moved with an accuracy of 0.01mm. Images were taken every 1mm over the entire range of the sliding plate to see the effect distance has on the resolution of the webcam. The images were used to measure the height of the light source and this was plotted against the distance from the webcam as seen in figure 32. It was found that the distance of the light source did not have an effect on the resolution. This was due to the errors increasing with the height as the light source was moved nearer the webcam. Near the webcam there was a ten pixel difference in size for every 1mm moved and a single standard deviation was 2 pixels. This meant that it was possible to see to 20% of 1mm so it should be possible to see a movement of 0.2mm. As the distance from the webcam increases a distance change of 1mm involves a movement of 5 pixels. However the errors in readings also drop, this time to 1 pixel, hence still allowing a resolution of 0.2mm.

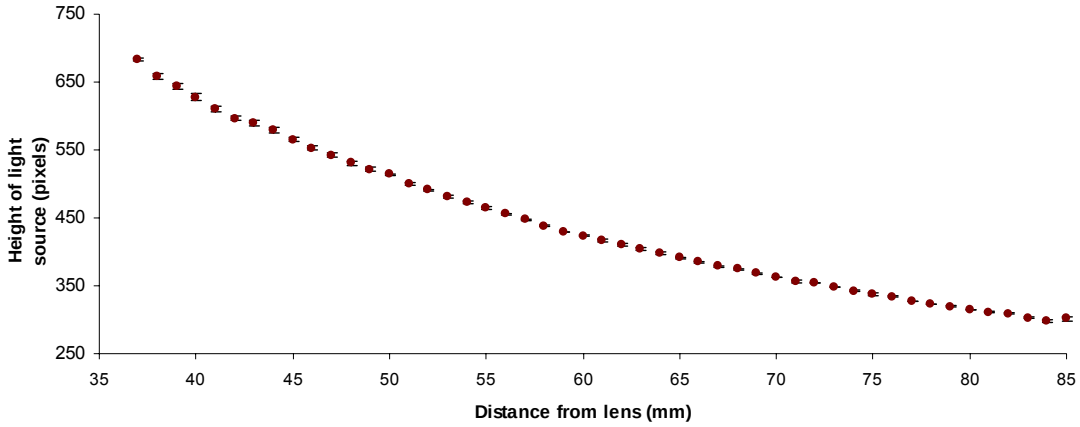

Figure 32: Graph showing the calibration data for the initial calibration of the webcam.

Once the calibration had been completed the angled laser beam meant that simple geometry could be used to determine the distance moved by the piezo actuator by knowing the angle of incidence on the mirror and the distance moved across the CCD. The basic geometry is shown in figure 33.

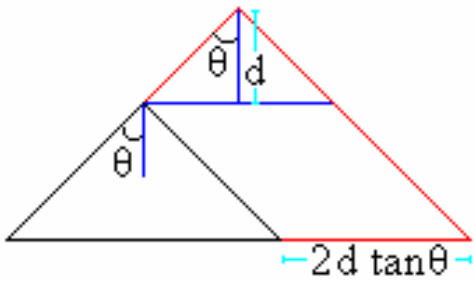

Figure 33: Geometry relating the distance moved across the CCD to the distance moved by the mirror.

As the webcam is parallel to the mirror it allows the distance moved by the mirror to be magnified by a factor of 2tanθ on the webcam. This has the advantage that the resolution of the camera does not have to be that of the mirror's movement, merely 2tanθ times the mirror's movement and the minimum requirement on the resolution can be increased by increasing the angle of incidence.

The equipment used for the original fine calibration imposed limitations on its effectiveness. These limitations were the resolution of the webcam, the fish-eye lenses limited sensitivity to small movements and the angle at which the laser beam was incident on the webcam.

The original calibration of the webcam was done using a fish-eye lens. However, the fish-eye lens meant that in order for the laser to be directly incident on the CCD then there was only a very narrow range of incident angles that could be used. Also,

when the piezo actuator was moved it was very difficult to see this change in the image produced as the light was channelled onto a narrow area of the CCD and so differences were easily lost. In order to try and rectify this problem it was decided to try removing the webcam's lens. This meant that the CCD could only see what was directly in front of it and an initial prediction was made that without the fish-eye lens on the webcam there would be a linear fit between the movement of the laser beam across the CCD and the movement of the laser dot on the image received. This was because the only lens in the system is used for focusing the laser beam onto the CCD and this should have no effect of the distance moved by the laser beam.

A recalibration of the webcam was then needed to account for the loss of the lens. This was done by placing the LVDT probe against the webcam and moving the webcam a set distance between images, as shown in figure 29. This was considered the equivalent of moving the laser beam across the stationary webcam and was significantly easier to achieve. This method was done twice to discover the motion of the laser beam across the CCD. The first measurement was taken to explore the large overall movement of the laser on the webcam whilst the second set of measurements were a more accurate measurement taken over a smaller range to determine to what accuracy it was possible to measure to.

In order to test the prediction that that without the fish-eye lens there would be a linear relationship between the distance moved by the webcam and the distance moved by the laser dot on the CCD data was taken at every 0.1mm over the length of the CCD. The results are shown in figure 34. They gave a smooth linear motion of the laser beam over the entire CCD and so confirmed the initial prediction.

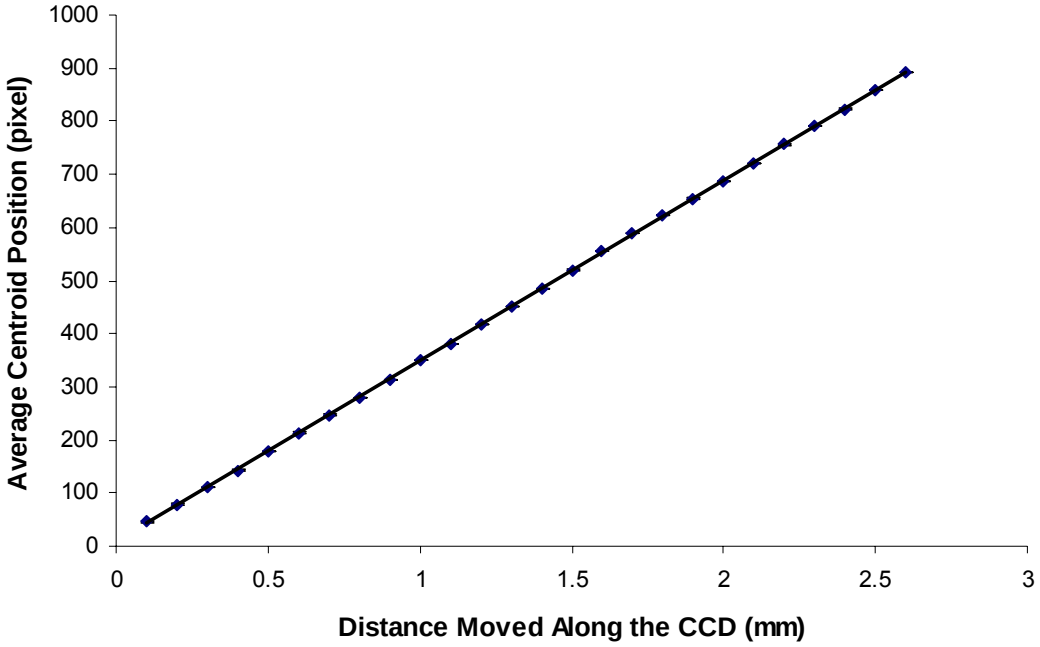

Figure 34: Graph showing the movement of the laser beam across the CCD.

To find the resolution of the camera, repeated results were taken over the central portion of the CCD as the response of the webcam was linear. A much smaller step size was used taking results every 0.01mm, the smallest distance it was possible to measure accurately to, for 0.1mm. Once these results had been converted into a

brightness graph by ImageJ the axial coordinates were moved into a curve fitting program in which Gaussian curves were fitted to the data points as seen in figure 35.

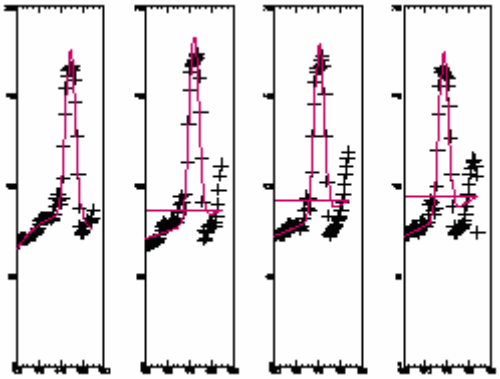

Figure 35: Plots of data points with Gaussian curves fitted. The black crosses are the original data points and the red line shows the computer fitted curves. The x-axis represents the distance along the CCD with the y-axis representing the gray value.

These curves allowed the peak of each graph to be found to better than one pixel and so give highly accurate results. These generated peaks were then plotted against each other to find the resolution as shown in figure 36.

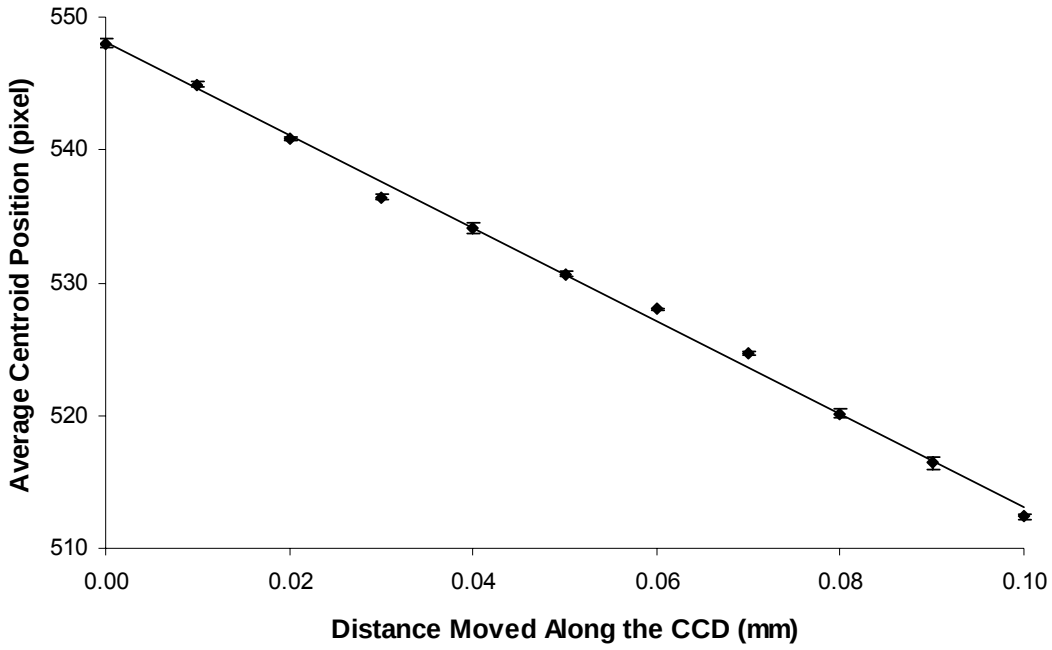

Figure 36: Graph showing the movement of the average centroid peak across the central portion of the CCD.

There is some deviation from the trend line but it is unknown whether this is due to the motion of the laser beam being not completely linear or whether it is from the LVDT probe being at its maximum accuracy and so giving small positioning errors. One standard deviation of the distance of the points from the line of best fit is 0.5 pixels. As a movement of 0.01mm occurs over a distance of 3.5 pixels this is equivalent to being able to see a movement of 1.5µm. As the Rayleigh Criterion gives a maximum resolution of 19µm for the webcam with its focusing lens, by putting

the data into the curve fitting program you are increasing the resolution of the system and so it is unlikely that this can be improved upon further.

Even with the removal of the fish-eye lens the angle at which the laser beam hit the CCD still caused problems. The greater the incident angle of the laser beam the larger the magnification of the mirror's movement. However, as can be seen in figure 37, the greater the incident angle the greater the cross sectional area seen by the CCD as the webcam is parallel to the mirror rather than perpendicular to the laser beam.

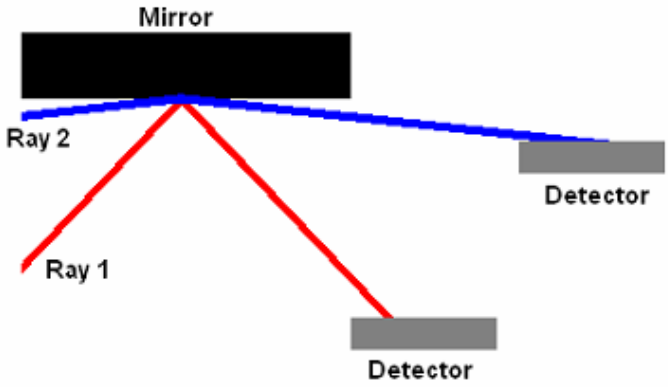

Figure 37: Incident rays on the CCD. Ray 1 has a small angle of incidence and so the cross section seen by the laser beam is little more than the laser beam's width. Ray 2 has a grazing incidence angle and the area seen by the CCD detector is much greater than that of the laser beam's width.

It was found experimentally that any incident angle greater than 20° gave too large a cross section on the CCD preventing a sharp enough peak being produced by the curve fitting software for position analysis. Unfortunately even using the maximum resolution possible this meant that it was not possible to get the camera to resolve the mirror's motion to 1μm. Due to this, photogrammetry techniques could not be used to create the alignment system. Instead interferometery techniques were looked into as it is known that these systems can easily see to 1μm.

2.2.3 Interferometry Design for Fine Piezo Actuator Calibration

As interferometry techniques measure to less than the wavelength of light only a simple interferometer was required and so a Michelson interferometer was created. Although they have the lowest accuracy it is still much larger than what is required for the calibration and it also has the advantage that it is easy to set-up and does not require expensive equipment.

In order to determine the distance moved by the piezo actuator it is necessary to count the fringes as they disappear or appear. The highest order fringes are at the centre of the pattern so it is easily seen when one appears or disappears. By counting the change in the number of rings the distance moved by the piezo actuator can be determined by

$$\Delta d = N(\lambda / 2), \qquad (7)$$

where Δd is the distance moved by the piezo actuator, N is the number of fringes that have disappeared and λ is the wavelength of light used. As this method gives an

accuracy of λ/2 it has the advantage that when it is placed in the cryostat it will be known that all noise is originating from the cryostat rather than from the alignment system.

To create the Michelson interferometer the equipment was assembled as shown in the diagram in figure 38 and an actual picture is given in figure 26.

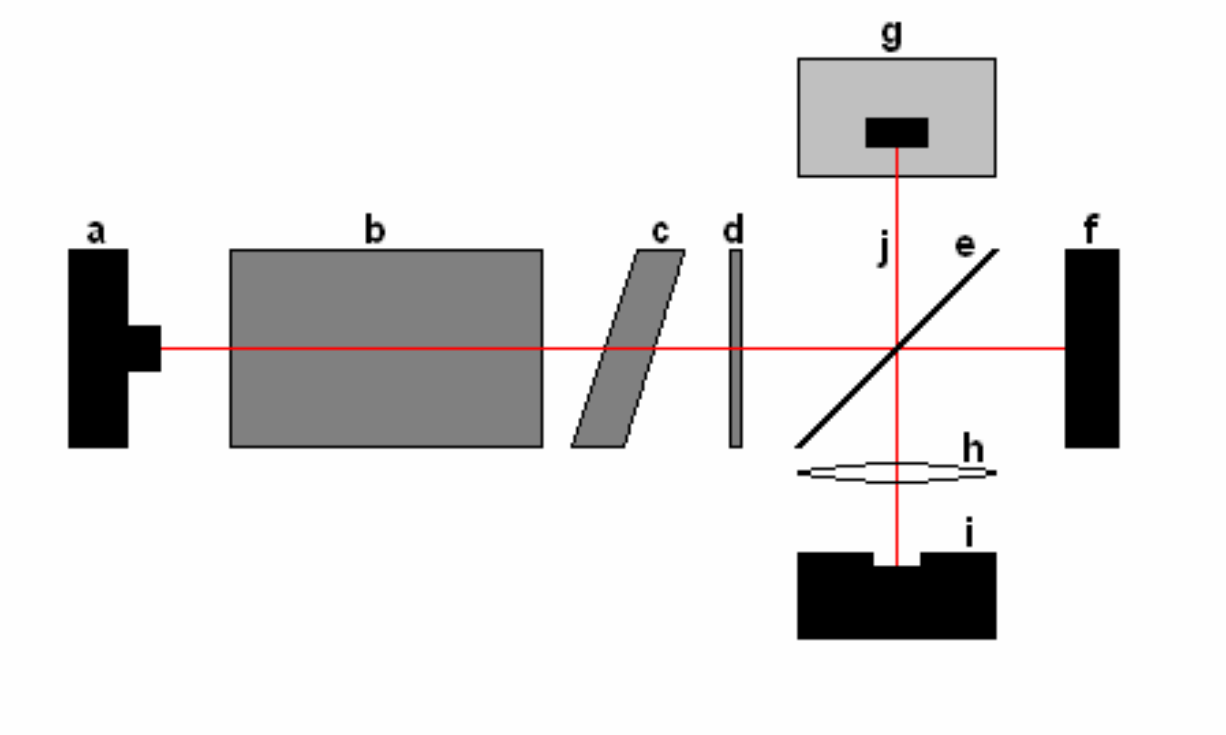

Figure 38: A diagram of the Michelson interferometer used. The labels are: a – laser, b – beam expander, c – polarizer, d – iris, e – half silvered mirror, f – full silvered mirror, g – piezo actuator with full silvered mirror mounted on top, h – lens, i – webcam

The laser light source was shone into a beam expander to increase the size of the laser beam and hence decrease the coherence of the beam. This was to try and increase the size of the interference pattern that would be seen by the CCD. The polarizer was needed to reduce the intensity of the beam in order to protect the CCD from saturation of the pixels. The iris was required to ensure that all the light entering the Michelson was parallel to the optical path. This ensured that only coherent light entered the interferometer.

The alignment of the Michelson took place in several stages. As the mirror mounted on the piezo actuator had very little freedom of movement, the other fixed mirror had to be aligned to the position of the piezo actuator. The half-slivered mirror was set at an angle of approximately 45°. The fixed mirror was covered preventing reflection and the piezo actuator and beamsplitter were aligned. This was achieved by noting the placement of the incident ray on the beamsplitter and comparing it to the position of the ray reflected from the piezo actuator. The beamsplitter was then moved to align both the incident and the reflected ray on top of each other. The mirror mounted on the piezo actuator was then covered and the fixed mirror was aligned. This was done in a similar manner to that of the piezo actuator but rather than manipulating the beamsplitter to align the incident and reflected rays the fixed mirror itself was moved. Once the incident beam and the reflected beam from the fixed mirror were aligned both mirrors were uncovered and the image produced on the

CCD was examined. From this the fixed mirror was then moved until the images from the piezo actuator and the fixed mirror were aligned exactly on top of each other. This gave an aligned Michelson interferometer.

Unfortunately no results were able to be obtained with this method. It is believed that this was due to the laser light source being too coherent. As the Michelson effectively Fourier transforms the input, a laser light source gives an extremely well defined and narrow output. This means that any small defects within the interferometer cause the fringe pattern to become hidden. In order to be able to see the fringes a source that gives a larger output signal is needed. For this a filtered white light source was used. This gives an input of a very narrow range of frequencies and outputs a large but complicated pattern. Despite its complexity the large size allows it to be seen easily. To accommodate the new light source the set-up was changed slightly with a diagram of it shown in figure 39 and a picture of it in figure 27.

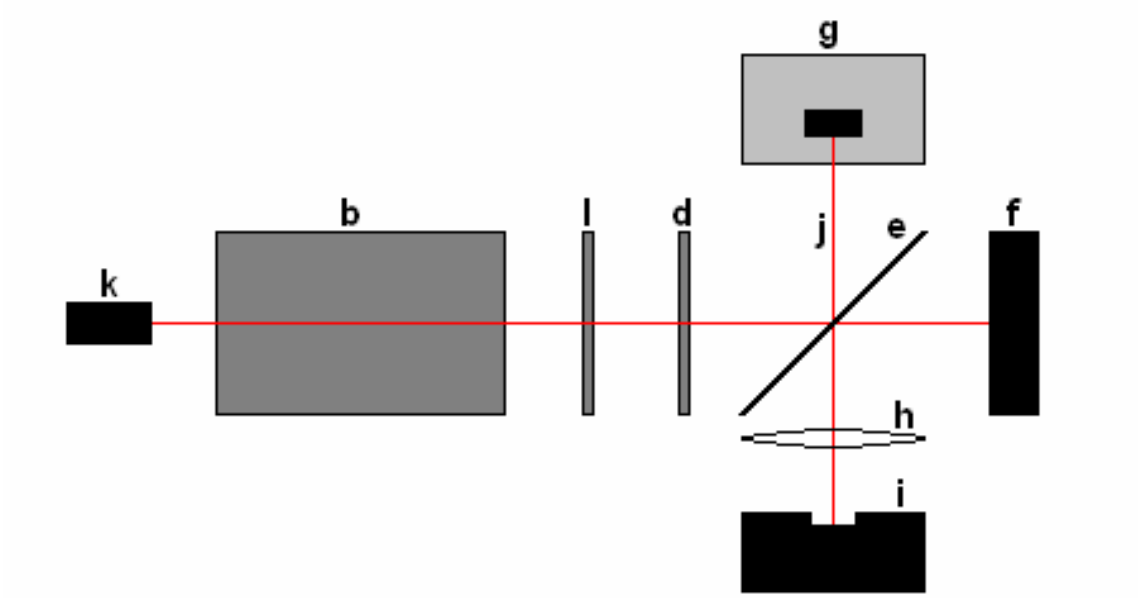

Figure 39: Diagram of the adapted Michelson interferometer. The labelling is as follows: b – beam expander, d – iris, e – half silvered mirror, f – full silvered mirror, g – piezo actuator with full silvered mirror mounted on top, h – lens, i – webcam, j – optical axis, k – white light source with red filter, l – second iris

Two irises are required to ensure that all the light entering the Michelson interferometer is parallel to the optical axis. When only one iris is used the light spreads outwards as a lot of scattered light passes through it. By using a second iris this scattered light is stopped from entering the interferometer.

3 Results and Interpretation

3.1 Initial Rough Piezo Actuator Calibration

The initial test to determine the piezo actuator's basic movement found that fifty steps gave an average of distance change of 0.02mm. Several anomalies were also found. The first occurs at the start of the piezo actuator's movement. For the first thousand steps there is a small increase of the step size. This is matched by a decrease in step size at the end of the piezo's movement. However, the decrease at the end is more likely due to unrepeatability in the number of steps taken in each expansion of the piezo actuator rather than due to sticking, which is the probable cause for the small step size at the start. In both cases these areas will have to be avoided when taking data to reduce systematic error. The dip in step size at the centre of the graph shown in figure 40 is believed to be caused by the set-up used rather than being an intrinsic feature of the piezo actuator, as when further readings were taken this feature did not exist. If the LVDT probe was not exactly perpendicular to the piezo actuator then a sideways force could cause a sticking force which slightly affects the results.

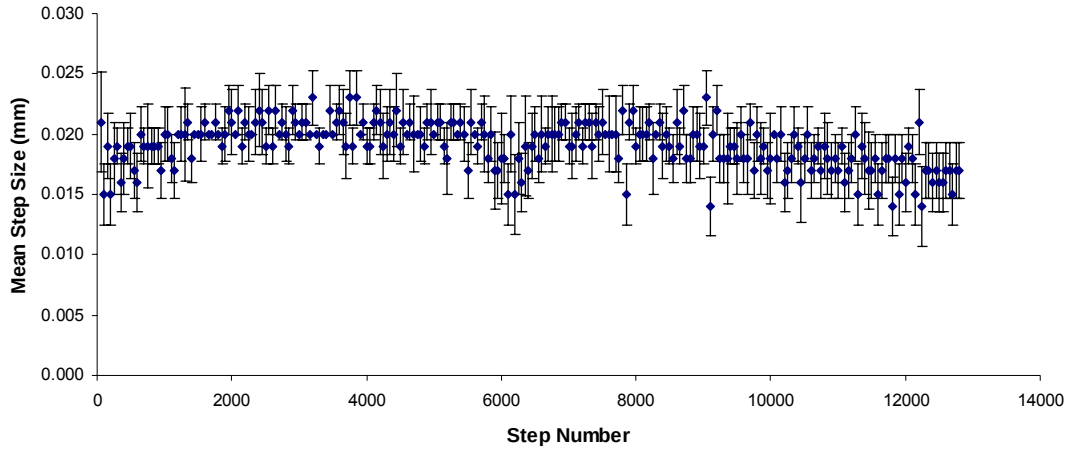

Figure 40: Graph showing the results of the change in step size as a function of the number of steps from the start.

3.2 Fine Piezo Actuator Calibration

When the two arms of the Michelson interferometer are at an equal distance from the beamsplitter the intensity of the generated image is increased. It is in this area that the fringe pattern is most easily seen. In order to find this zero path difference area it was necessary to run out the piezo actuator over its entire linear range. Images were taken at regular intervals and their brightness plotted against the distance moved by the piezo actuator. The resultant graph is shown below in figure 41. The increase in intensity is clearly seen between 4000 and 5000 steps.

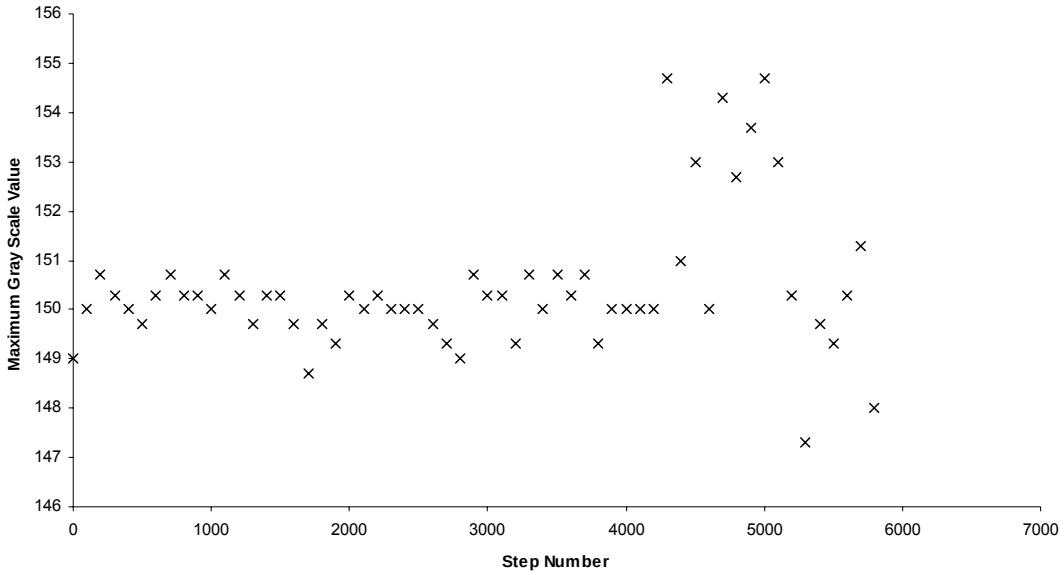

Figure 41: Graph showing the position of zero path difference.

The area of zero path difference was then looked at using a higher sampling rate. This was needed to see the fringe pattern. The results are shown in figure 42.

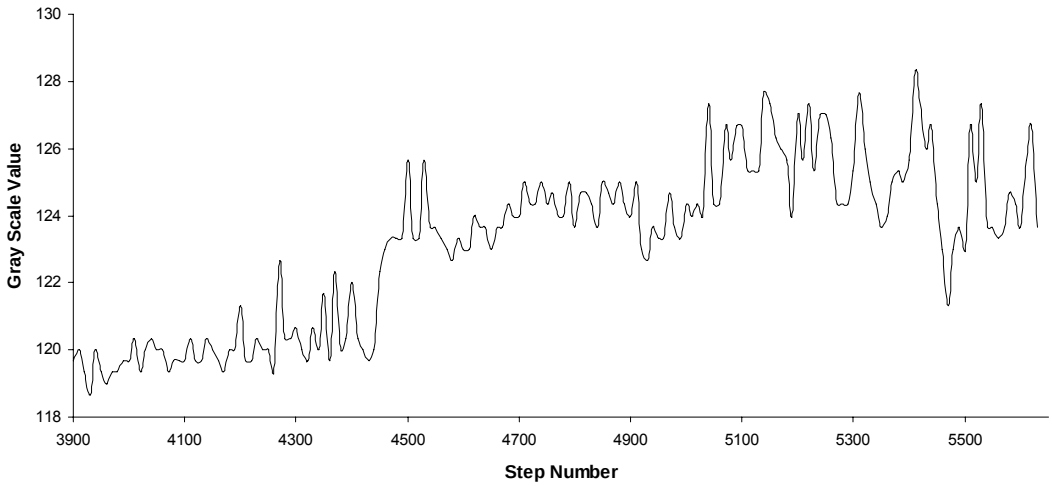

Figure 42: Graph of the zero path difference area.

From figure 42 it can be seen that the expected pattern as shown in figure 9 is not visible. This is probably due to the large step size relative to the wavelength of light that was used. This resulted in under sampling of the data. In order to try and rectify this, the step size of the piezo actuator needs to be reduced. According the manual for the attocube piezo actuators there is a linear relationship between the voltage placed across the piezoelectric crystal and the step size of the piezo actuator.

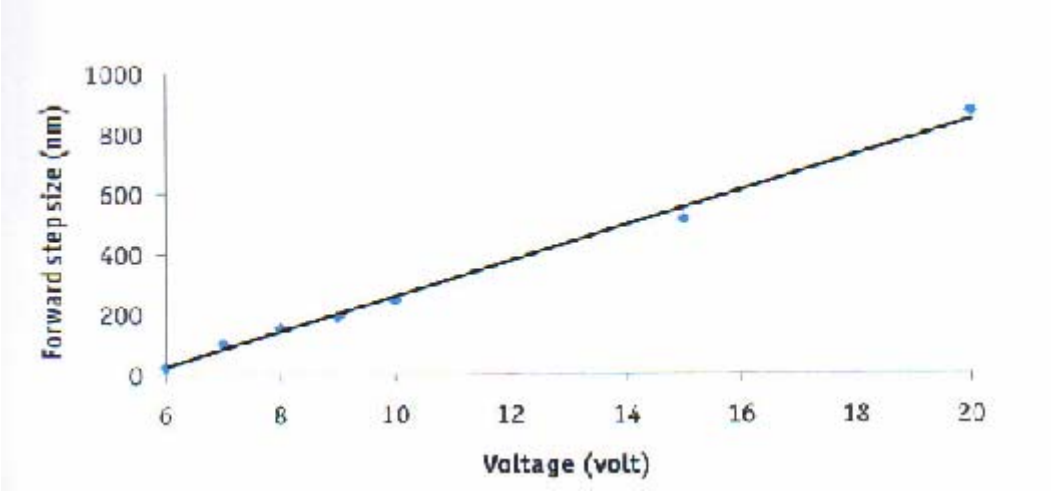

Figure 43: Manufacture's results for the movement of the piezo actuator.

As seen in figure 43, to quarter the step size of the piezo actuator from an initial voltage input of 20V a reduction by 12V is needed. So by applied 8V a step size of 100nm should be acquired. However, the piezo actuator is taking smaller step sizes at 20V than the value given by the manual. This may mean that reducing the voltage by 12V may not produce the same drop in step size. Unfortunately due to time constraints it was not possible to repeat the rough calibration and so it was assumed that the step was reduced to 100nm by lowering the voltage to 8V, although in analysing the results it's important to remember that this may not hold true.

A short section of the zero path difference area was re-examined with this smaller step size allowing a higher sampling rate. The maximum brightness at each step was again plotted against the movement of the piezo actuator. These results are shown in figure 44.

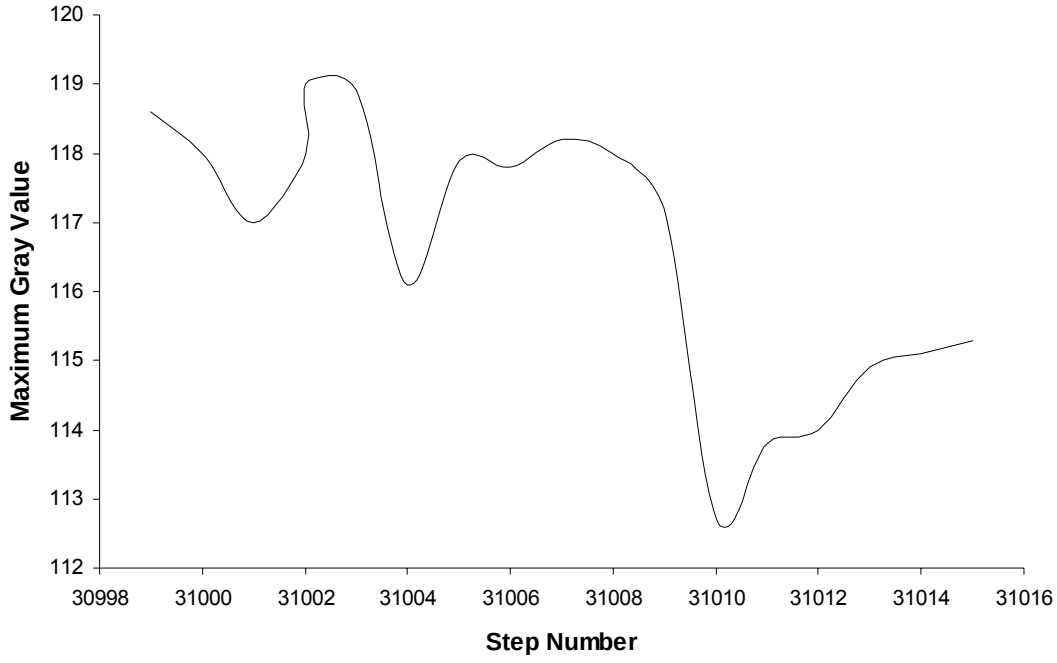

Figure 44: Graph showing the zero path difference area with a small sample rate.

As the step size is 100nm and the wavelength of light is approximately 600nm there should be six fringes as the spacing between peaks is half of the wavelength of the light. There appears to be three possible peaks although the non-uniform shape and spacing makes them unsuitable for alignment purposes. It is possible that the data sampling rate is still too low to allow a clear view of the fringe pattern. It is also possible that the cross-section through the light incident on the detector is not taken at the exact centre. This would obscure results as the maximum peak would never be reached. A final possibility is that expected pattern has been shifted lowering the intensity where a peak would be expected.

This shifting of the output can be caused by a change of polarisation of light or phase changes occurring within the system. The polarisation of light affects the intensity at a given position after recombination by

$$I = \left\langle E_{P_1} \middle| E^*_{P_2} \right\rangle \tag{8}$$

where I is the intensity of light a given point, E_{P_1} is the polarisation wave 1 and $E^*_{P_2}$ is the polarisation of wave 2. Equation 8 gives a maximum when the polarisation from both arms equal each other. If the two polarisations are orthogonal to each other then the output intensity is zero. This means that if one of the waves had its polarisation altered slightly during reflection the resultant intensity would be lower than expected. Rough reflecting surfaces can cause phase shifts within a wave. These will be constant and so when the two waves are recombined then there is a constant phase shift. A constant phase shift also arises from a lack of a compensator plate in the interferometer. This causes one wave to remain in the glass for longer than the other, delaying it slightly.

As all these factors combine to reduce the fringe pattern rather than eliminate it, it is possible that there may still be a fringe pattern within the results but it is obscured by the scalar recombination of the light wave. In order to try and see the fringe pattern it was necessary to remove the background scalar recombination from the image taken by the webcam. This was achieved by taking an image at the furthest point possible from the zero path difference area, so would have the smallest fringe pattern on it, to be used as the background image. The background image was then removed from an image taken within the zero path difference area. The resultant brightness can be seen below in figure 45.

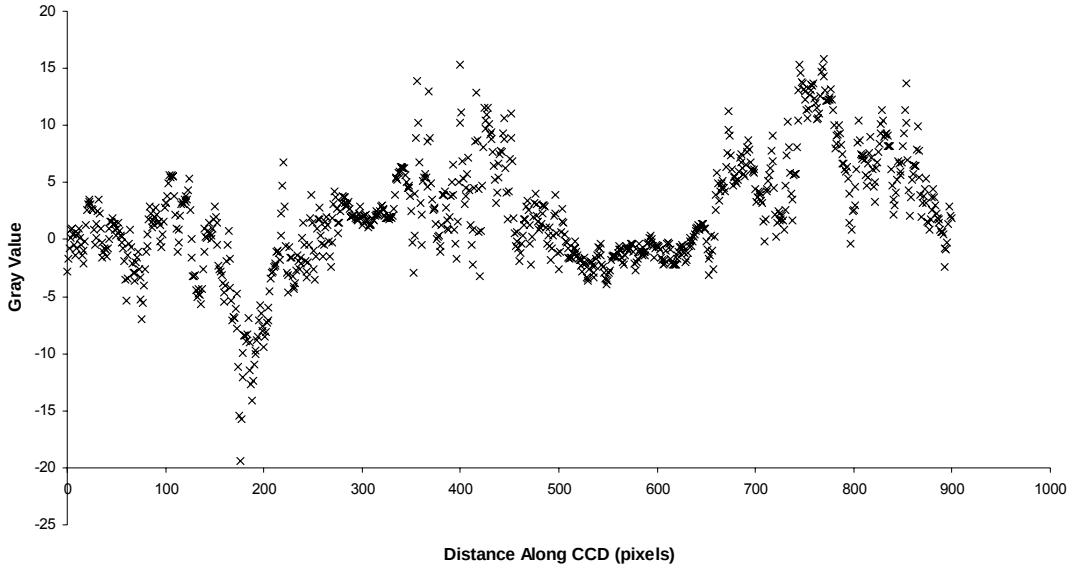

Figure 45: Graph of resultant when a background image is removed from an image taken inside the zero path difference area.

The oscillations in brightness are a cross section through a fringe pattern. However they do not change with the movement of the piezo actuator and so are a spatial fringe pattern originating from the mirrors not being perfectly parallel to each other, as discussed in section 1.6.

If the position of the cross section taken though the image was not along the exact centre then the resultant brightness would not reach its potential maximum and so skewering results. To see if this was affecting the results the total intensity of the entirety of the incident light was found by taking its integrated density. The integrated density is simply the sum of all the brightness pixels with in a given area[30]. Figures 46 and 47 show the difference in the area used.

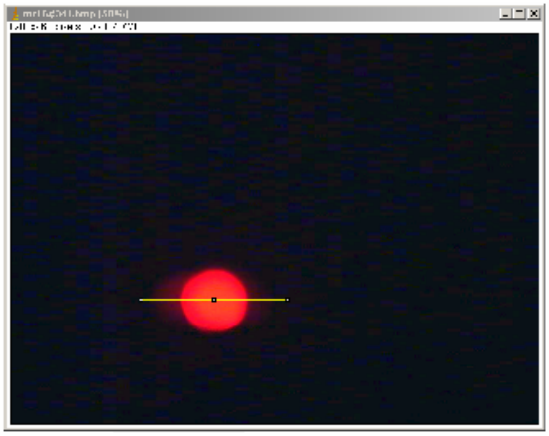

Figure 46: Cross section through the incident light.

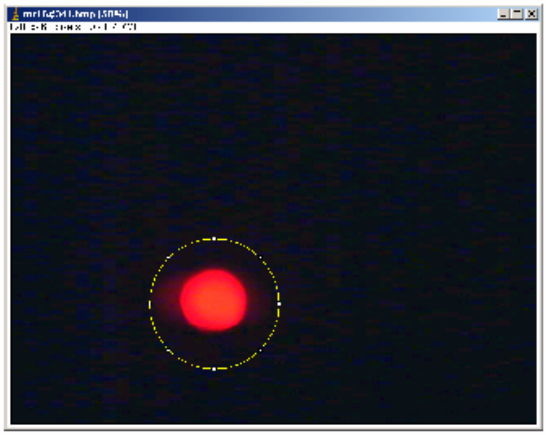

Figure 47: Area over which the integrated density was taken.

When the integrated density was plotted against the movement of the piezo actuator, a fringe pattern emerged as shown in figure 48. There are five definite peaks, one of which seems to be two peaks combined. The spacing of the peaks are two to three steps apart. With a wavelength of 600nm the spacing between peaks should be

300nm and so this ties in with the approximate step size of 100nm. This fringe pattern shows that taking a cross section was affecting the results and so in any further work the integrated density should be used.

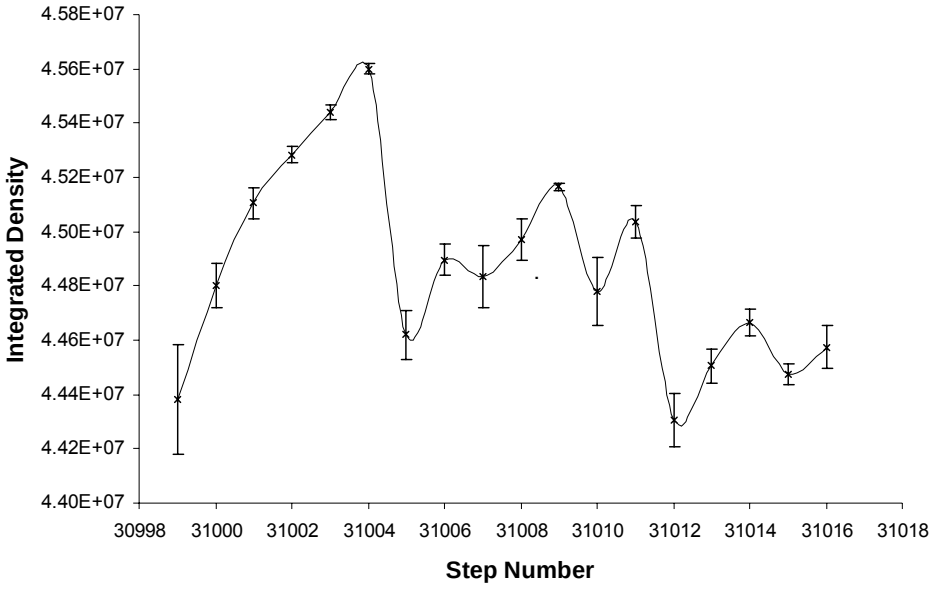

Figure 48: Zero path difference area looked at using a small sample rate and the integrated density.

4 Future Work

The work detailed in this report needs building on to reach its final stage. A very fine step size is required by the piezo actuator to be able to see the fringes and this needs to be perfected first. Once the ideal step size has been found changes can be made to try and increase the contrast of these fringes.

All of the webcam's software is still running and it maybe possible that it is reducing fluctuations in the image presented on the screen. To protect against this the webcam needs to be replaced by a photo diode. This will ensure that all the data from the interferometer is being captured and processed.

A compensator plate and polarisers should also be added to the interferometer. The compensator plate would help to reduce the phase difference between the waves coming from separate arms improving interference. Polarisers need to be added to both arms of the interferometer to ensure that the polarisation of the light does not rotate, allowing maximum intensity output.

Once the Michelson interferometer has been perfected it then needs to be cryogenically cooled for the final calibration. As the piezo actuator cools its step sizes will decrease as the distance the atoms move become shorter due to contraction from the cold. The set-up for the cryogenic system is shown in figure 49, where the Michelson interferometer is inside the cryostat with the light source

entering from outside the cryostat through a window and exiting to a detector outside, again through a window in the cryostat.

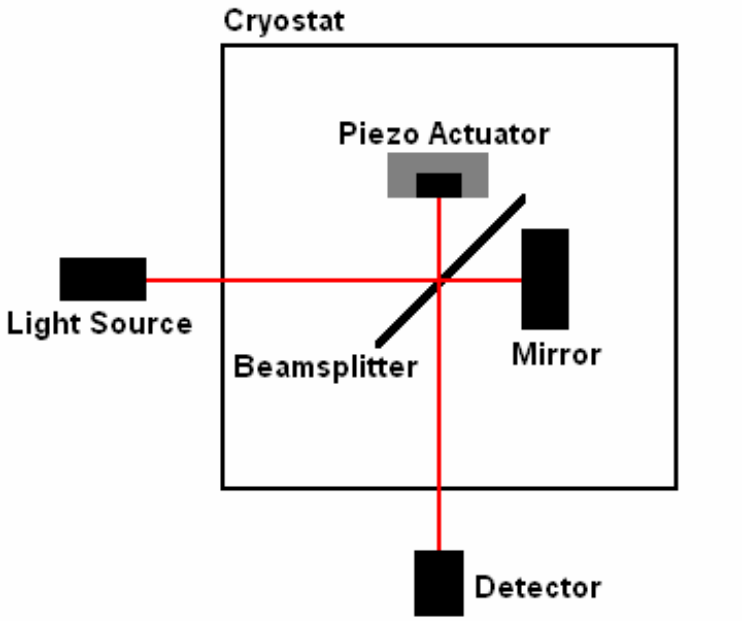

Figure 49: Set-up required for the cryogenic calibration of the piezo actuator.

Once the cryogenic calibration of the piezo actuator has been completed the detector can be replaced by the fibre optic sensors to allow for their calibration.

5 Conclusions

It has been found that whilst photogrammetry techniques can be improved upon to gain an accuracy of 1.5μm it is not possible to use them for work requiring a minimum accuracy of 1μm. For alignment systems working over this region it is necessary to use a laser based system. Interferometry has a much higher accuracy allowing the advantage of knowing that any noise present in the results is not due to the alignment system. However, even the relatively simple systems take time to assemble and align correctly and more work is required to turn the current system in a functioning alignment system.

6 Acknowledgements

My gratitude goes out to Professor Bruce Swinyard for his continual help in the construction of my alignment device, his support in getting it to work, his guidance in the development of my project and continual encouragement throughout this project.

I would like to thank Dr Marc Ferlet for his amazing knowledge on optical systems, the generous use of his equipment and his ability to find whatever piece of equipment was needed. My thanks also go to Dr Karen Aplin for the kind use of her lab and cheerful help.

I also need to thank both Dr Clive Speake and Dr Andrzej Fludra for organising this year and allowing me to attend Rutherford Appleton Laboratories. Thank you also to Dr Fludra for immense help with the organising of the lectures and remarkably quick

feedback on assessed work. Thanks also need to go to Dr Speake for his guidance and support throughout this project.

8 Appendix

Figure A50: (a) LVDT Probe

Figure A51: (b) Piezo Actuator

Figure A52: (c) Laser Light Source

Figure A53: (d) Webcam

Figure A54: (e) Piezo Actuator with Mounted Mirror

Figure A55: (f) Beam Expander

Figure A57: (h) Polarizer

Figure A56: (g) Ground Glass

Figure A58: (i) Iris

Figure A59: (j) Beamsplitter

Figure A61: (l) Focusing Lens

Figure A60: (k) Full Slivered Mirror

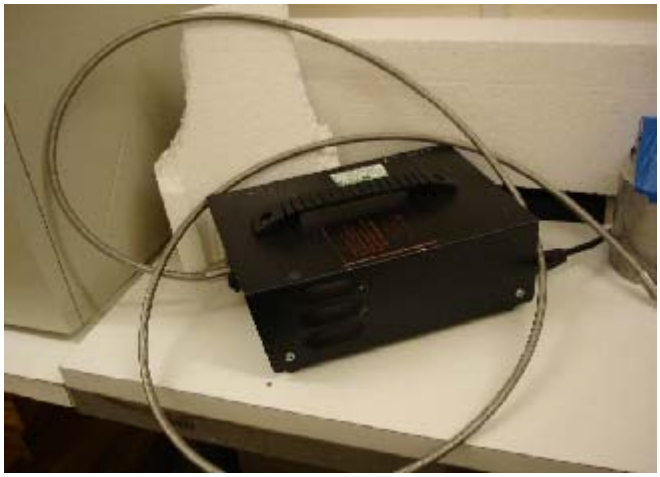

Figure A62: (m) White Light Source

Figure A63: (n) Second Iris

Figure A64: (o) LED Light Source

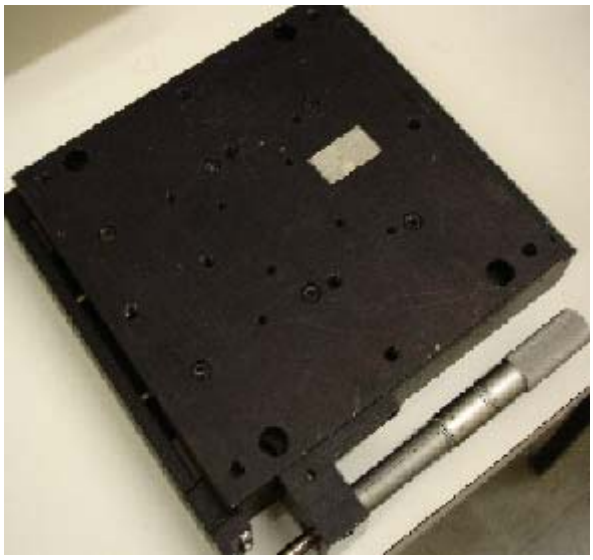

Figure A65: (p) Sliding Plate

7 References

[1] http://jwst.gsfc.nasa.gov/about.html Current on 04/12/06

[2] http://ircamera.as.arizona.edu/MIRI/page2.htm Current on 04/10/06
[3] Philtec, Fibreoptic Displacement Sensors – Non-contact sensing for demanding applications, Product Catalog 2002
[4] Boudreau R. (1997) *Passive optical alignment methods* (1997 International Symposium on Advanced Packaging Materials)
[5] Courtesy of Chris Price and Chang *et al* (1993) *Calibrating a mobile camera's parameters* (J. Pattern Recognition Soc., Vol. 26, Pages 77-88)
[6] Rank Taylor Hobson Limited (1984) *'Optical Alignment With the Talyor-Hobson Micro-Alignment Telescope and its Accessories'*
[7] Salvi J., Armangué X. & Batlle J. (2002) *A comparative review of camera calibrating methods with accuracy evaluation* (J. Pattern Recognition Soc., Vol. 35, Pages 1617-1635)
[8] Ayliffe M. H., Châteauneuf M., Rolston D. R., Kirk A. G. & Plant D. V. (2001) *Six-degrees-of-freedom alignment of two-dimensional array components by use of off-axis linear Fresnel zone plates* (Applied Optics, Vol. 40, Pages 6515-6526)
[9] http://scienceworld.wolfram.com/physics/MichelsonInterferometer.html Current on 14/02/07
[10] http://science.howstuffworks.com/question421.htm Current on 14/02/07
[11] www.numbera.com/musictheory/mechanics/physics.aspx Current on 14/02/07
[12] www.search.com/reference/Interference Current on 20/03/07
[13] Hecht E. (2002) *Optics* (Fourth International Edition, Addison Wesley, San Francisco)
[14] Champeney D. C. (1973) *Fourir transforms and their physical applications*
[15] Walter K. (1997) *New Interformeter Measures to Atomic Dimensions* (Science and Technology Review, Oct 1997, Pages 6-7)
[16] Philtec Fiberoptic Displacement sensors – Non-contact sensing for demanding applications, Product Catalog 2002
[17] Salvi J., Armangué X. & Batlle J. (2002) *A comparative review of camera calibrating methods with accuracy evaluation* (J. Pattern Recognition Soc., Vol. 35, Pages 1617-1635)
[18] Zhang Z. & Pan Z. (2004) *Three-dimensional measurement with use of a single camera* (Applied Optics, Vol.43, Pages 2449-2455)
[19]Iovenitti P., Thompson W. & Singh M. (1996) *Three-dimensional measurement using a single image* (Optical Engineering, Vol. 35, Pages1496-1502)
[20] Châteauneuf M. & Kirk A. G. (2004) *Six-degrees-of-freedom alignment technique that provides diagnostic misalignment information* (Applied Optics, Vol. 43, Pages 2689-2694)
[21] Li S., Yang C., Zhang E. & Jin G. (2005) *Compact optical roll-angle sensor with large measurement range and high sensitivity* (Optics Letters, Vol.30, Pages 242-244)
[22] Liu C., Jywe W. & Tzeng S. C. (2004) *Simple three-dimensional laser angle sensor for three-dimensional small-angle measurements* (Applied Optics, Vol. 43, Pages 2840-2845)
[23] Jahns J. & Däschner W. (1992) *Precise alignment through thick wafers using an optical copying technique* (Optics Letters, Vol. 17 Pages 390-392)
[24] www.doitpoms.ac.uk/tlplib/optical-microscopy/resolution.php Current on 14/02/07
[25] Shah S. & Aggarwal J. K. (1996) Intrinsic parameter calibration procedure for a (high-distortion) fish-eye lens camera with a distortion model and accuracy estimation (Pattern Recognition Society, Vol.29, Pages 1775-1788)
[26] www.answers.com/topic/piezoelectricity Current on 21/02/07
[27] C. Kittel, *Introduction to Solid State Physics*, 5th ed., 1976, John Wiley & Sons Inc.
[28] attocube systems, User Manual, Inertial XYZ Positioner, ANPxyz100, Version: 1.5, Modified: January 05
[29] www.cambridgeincolour.com/tutorials/color-black-white.htm Current on 18/03/07
[30]66.102.9.104/search?q=cache:6qPJlWxiExYJirsb.info.nih.gov/ij/docs/menus/analyze.html+define+%22intergrated+density%22+intensity&hl=en&ct=clnk&cd=8&gl=uk Current on 28/03/07